Flamingo participates in multiple models of cell competition

Pablo Sanchez Bosch[1,2], Bomsoo Cho[1,2], Jeffrey D. Axelrod[1*]

1. Department of Pathology, Stanford University School of Medicine, 300 Pasteur Dr., Stanford CA, 94305, USA
2. These authors made equal contributions.

* Corresponding author

Abstract

The growth and survival of cells with different fitness, such as those with a proliferative advantage or a deleterious mutation, is controlled through cell competition. During development, cell competition enables healthy cells to eliminate less fit cells that could jeopardize tissue integrity, and facilitates the elimination of pre-malignant cells by healthy cells as a surveillance mechanism to prevent oncogenesis. Malignant cells also benefit from cell competition to promote their expansion. Despite its ubiquitous presence, the mechanisms governing cell competition, particularly those common to developmental competition and tumorigenesis, are poorly understood. Here, we show that in *Drosophila*, the planar cell polarity (PCP) protein Flamingo (Fmi) is required by winners to maintain their status during cell competition in malignant tumors to overtake healthy tissue, in early pre-malignant cells when they overproliferate among wildtype cells, in healthy cells when they later eliminate pre-malignant cells, and by supercompetitors as they compete to occupy excessive territory within wildtype tissues. "Would-be" winners that lack Fmi are unable to over-proliferate, and instead become losers. We demonstrate that the role of Fmi in cell competition is independent of PCP, and that it uses a distinct mechanism that may more closely resemble one used in other less well-defined functions of Fmi.

Introduction

Dividing cells in proliferative tissues must maintain tissue homeostasis and structural integrity as well as preserve their genetic integrity. One of the mechanisms operating in proliferative tissues to achieve these requirements is cell competition. Cell competition is a process in which cells of a higher fitness ("winners") eliminate less fit neighbors ("losers"), by inducing cell death (Norman et al., 2012; Meyer et al., 2014; Di Giacomo et al., 2017; Watanabe et al., 2018) and/or extrusion from the epithelial layer (Norman et al., 2012; Kon et al., 2017; Kohashi et al., 2021). Cell competition was first recognized in 1975 (Morata & Ripoll, 1975), when Morata and Ripoll studied the growth of *Drosophila* carrying a mutation in the gene for the ribosomal protein RpS17 (termed *minute*). Animals heterozygous for this

minute mutation are viable but develop slowly due to decreased proliferation rates. They further observed that clones of cells carrying this *minute* mutation in a wildtype background were eliminated from the *Drosophila* developing wing. Since then, extensive advances have been made in our understanding of the process (reviewed in (Morata, 2021)). We now know that cell competition can be triggered by mutations that cause a disadvantage, such as the aforementioned *minute* cells, and can also be triggered by mutations that confer a proliferative advantage, such as ectopic expression of proto-oncogenes such as Myc or Ras (Moreno & Basler, 2004; de la Cova et al., 2004; Hogan et al., 2009). In this case, the process is known as super-competition, and wildtype cells behave as losers and are eliminated from the tissue by the mutant super-competitors. The "survival of the fittest" effect observed in cell competition has been shown to be critical during embryonic and larval development as well as for tissue homeostasis (Amoyel & Bach, 2014; Maruyama & Fujita, 2017; Morata, 2021). Much additional research has shown that cells and their neighbors are constantly evaluating their fitness, and that the active elimination of less fit cells is critical to maintain tissue integrity (Ellis et al., 2019), maintain chromosomal stability (Baillon et al., 2018; Ji et al., 2021), ameliorate effects of cellular aging (Merino et al., 2015) and suppress tumorigenesis (Kon et al., 2017; de Vreede et al., 2022).

While cell competition has been observed in many cell types, much attention has focused on studies in epithelia (Vincent et al., 2013). Polarity is a hallmark of epithelial tissues, and loss of polarity plays a prominent role in triggering cell competition and in the process of eliminating loser cells. Cells harboring mutations in apicobasal polarity genes have been shown to induce and/or regulate cell competition when surrounded by wildtype cells. In *Drosophila*, mutations in apicobasal polarity genes *scribble* (*scrib*), *discs large* (*dlg*), and *lethal giant larva* (*lgl*) all trigger cell competition when induced clonally (i.e. surrounded by wildtype cells), and the clones are eliminated from the epithelial tissue (Hariharan & Bilder, 2006; Morata & Calleja, 2020). However, clones that are deficient for any of these polarity genes can survive if they are competing against less fit cells, or if they carry additional mutations that confer a growth advantage. For example, when *lgl* clones, which would be eliminated when surrounded by wildtype cells, are made to express elevated levels of Myc, the competition is reversed, and they instead become winners (Froldi et al., 2010). This context-dependence and fitness surveillance highlights the complexity of cell competition and its plasticity.

In epithelial tissues, cell competition is critical to suppress tumorigenesis, as polarity-deficient clones are prone to malignancy. When *scrib* mutant epithelial cells acquire elevated activity of a proto-oncogene such as the constitutively active Ras^{V12}, these clones acquire malignant properties of ectopic growth and invasiveness (Pagliarini & Xu, 2003; Brumby & Richardson, 2003). Surveillance and rapid elimination of cells that develop polarity defects therefore serves to protect epithelia from oncogenesis. This competitive mechanism is known as Epithelial Defense Against Cancer, or EDAC (Maruyama & Fujita, 2017; Kon & Fujita, 2021). Through EDAC, normal epithelial cells eliminate neighboring transformed cells by inducing apoptosis or by inducing their apical or basal extrusion from the epithelial layer (Watanabe et al., 2018; Kohashi et al., 2021) . On the other hand, tumors that exhibit more aggressive properties and escape the defense mechanisms not only proliferate but actively engage in cell competition to promote their own growth and malignancy (Vishwakarma & Piddini, 2020; Madan et al., 2022). For example, growth of *Drosophila* $APC^{-/-}$ intestinal adenomas requires active elimination of wildtype cells, and inhibiting cell death in the wildtype tissue hampers adenoma growth (Suijkerbuijk et al., 2016).

In addition to apicobasal polarity, epithelial tissues are planar polarized. Planar cell polarity (PCP) signaling polarizes cells within the plane of the epithelium to orient cellular structures, cell divisions, and

cell migration during development and homeostasis (Adler, 2002; Simons & Mlodzik, 2008; Vladar et al., 2009; Butler & Wallingford, 2017). Intercellular Fmi homodimers scaffold the assembly of a set of core PCP proteins: on one side of a cell, Frizzled (Fz), Dishevelled (Dsh), and Diego (Dgo) comprise a complex that interacts with another complex containing Van Gogh (Vang) and Prickle (Pk) on the opposite side of the adjacent cell. Fmi homodimers transmit differential signals in opposite directions to communicate the presence of either protein complex to the other, linking the proximal and distal complexes and mediating asymmetric signaling between them (Lawrence et al., 2004; Strutt & Strutt, 2007; Strutt & Strutt, 2008; Chen et al., 2008; Struhl et al., 2012). In addition to establishing planar polarity, numerous reports have suggested links between PCP signaling and cancer progression, promoting cell motility, invasiveness and metastasis (Weeraratna et al., 2002; Katoh, 2005; Katoh & Katoh, 2007; Coyle et al., 2008; Gujral et al., 2014; VanderVorst et al., 2018; VanderVorst et al., 2023). Its roles, however, remain poorly characterized.

To probe a potential connection between PCP and cancer, we employed a *Drosophila* eye tumor model. We discovered a requirement for Fmi, but not other core PCP proteins, in tumor associated cell competition. We found that aggressive tumors require Fmi to outcompete the neighboring wildtype tissue. We then found that this Fmi requirement is not unique to tumor competition; in several developmental cell competition scenarios, removing Fmi from winner cells prevents them from eliminating their neighbors and transforms them into losers. “Would be” winners that lack Fmi show both a decrease in proliferation and an increase in apoptosis. By several criteria, we show that this function for Fmi is independent of its role in PCP signaling.

Results

Flamingo is required for tumorigenesis in Drosophila Ras^{V12} tumors

Planar polarity has been linked to tumorigenesis in several organisms, tumor models, and patient tumor samples (Kaucká et al., 2013; Asad et al., 2014; Puvirajesinghe et al., 2016; VanderVorst et al., 2018; Chen et al., 2021c; Li et al., 2021; Chen et al., 2021b). We explored how the core PCP complex might be involved in tumorigenesis. To do so, we used the versatile and widely used Ras^{V12} tumor model in *Drosophila* eye imaginal discs. In this model, eye disc cells are transformed into highly tumorigenic cells by co-expressing the constitutively active Ras^{V12} oncoprotein and RNAi against the tumor suppressor Scribble (Scrib) (Pagliarini & Xu, 2003). Cells expressing these genes quickly expand into massive tumors and invade the neighboring brain tissue (Fig 1A-C).

To study the requirement for PCP signaling in tumors, we expressed *Ras^{V12}* and *scrib* RNAi throughout the eye, and simultaneously down-regulated PCP core proteins by also expressing validated RNAi’s against *fmi*, *fz*, *dsh*, *vang*, and *pk*. We then imaged tumor size through the pupal cuticle. We observed that tumor growth was unaffected by knockdown of any of the core PCP genes at third instar larval or at early pupal stages (Fig 1A-H). We then asked whether PCP signaling might be required by tumors when they’re confronted by wildtype cells. To test this hypothesis, we created clonal tumors in the eye disc by expressing *Ras^{V12}* and *scrib* RNAi under control of ey-Flp. In this model, nearly every cell in the eye disc will perform chromosomal recombination (Fig 1 Suppl 1), producing an eye disc composed of approximately 50% wildtype and 50% tumor cells. Under these conditions, tumor cells expand aggressively, displacing wildtype cells and causing massive overgrowth of the eye disc and metastasis to

the larval brain (Fig 1I-K). We created clonal tumors that were also null for either *fmi*, *fz*, *dgo*, *vang*, or *pk* and evaluated them for their ability to grow and metastasize when confronted with wildtype cells (Fig 1I-P). Remarkably, only *fmi* interfered with tumorigenesis, restraining growth of tumors in the eye disc and preventing them from invading neighboring tissues (Fig 1L). To ensure that the growth inhibitory effect of loss of Fmi in clonal tumors but not in whole eye tumors was not a result from comparing a null allele in clonal tumors vs RNAi in whole eye tumors, we generated *fmi* RNAi clonal tumors and compared them to control RNAi clonal tumors. While the effect was not as dramatic as with null clones, the size of *fmi* RNAi clonal tumors was substantially reduced compared to that of clonal tumors expressing *w* RNAi (Fig 1 Suppl 2A-B). Therefore, the same partial level of fmi knockdown impairs clonal tumor growth but not growth of whole eye tumors.

We also wished to directly compare growth of *fmi*-null clonal and *fmi*-null whole eye tumors. Because *fmi* alleles are embryonic lethal, we generated *fmi*-null tumors while eliminating WT cells from the eye disc using the GMR-Hid, l(2)CL system (Stowers & Schwarz, 1999). While *fmi*-null clonal tumors showed restrained growth (Fig 1L), elimination of WT cells in eye discs removed competition, and *fmi*-null tumors grew to a size comparable to control whole eye tumors (Fig 1 Suppl 2C-D). Because the effect of *fmi* was only apparent when tumors were induced in juxtaposition to wildtype cells, we hypothesized that Fmi may only be required in tumors that undergo cell competition.

Flamingo is required in winner cells during cell competition

Molecular mechanisms used by tumors in cell competition are sometimes shared by developmental cell competition. Malignant cells have been shown to actively eliminate surrounding cells by mechanical cell competition, apoptosis and engulfment (Levayer et al., 2016; Kohashi et al., 2021), similar to the cell-death mediated elimination of losers during developmental cell competition and EDAC (Maruyama & Fujita, 2017; Parker et al., 2021) Induction of JNK-mediated cell death is also common to developmental competition and tumor cell competition, as shown in intestinal adenomas (Suijkerbuijk et al., 2016). We hypothesized that the requirement of Fmi by competing tumors might also be shared in developmental cell competition. We therefore evaluated the role of Fmi in non-malignant, developmental cell competition models.

Cells expressing high levels of Myc behave as winners when growing among wildtype cells, proliferating faster than wildtype cells and inducing their elimination. Despite Myc being a proto-oncogene, in contrast to Ras^{V12} *scrib* RNAi tumors, Myc overexpressing clones do not become tumors, but instead expand to occupy larger than normal domains of morphologically normal tissue (Moreno & Basler, 2004; de la Cova et al., 2004; Clavería et al., 2013). As for the Ras^{V12} *scrib* RNAi tumor model, we used UAS-myc and ey-Flp to create eye discs comprising initially equal populations of Myc overexpressing (>>Myc) and wildtype cells. As expected, >>Myc cells behaved like super-competitors, and the majority of cells (~65%) in late third instar discs were >>Myc cells (Fig 2A). However, when >>Myc cells were depleted of *fmi*, they failed to outcompete wildtype cells and behaved as one would expect of losers; the >>Myc, $fmi^{-/-}$ cells were outcompeted by wildtype cells such that late third instar eye discs were composed of only ~35% >>Myc, $fmi^{-/-}$ cells, suggesting that wildtype cells behave as winners against >>Myc, $fmi^{-/-}$ cells (Fig 2B,D). We then tested whether Fmi had an effect in the losers during >>Myc competition. Removing Fmi from the WT losers had no effect on this competition, as >>Myc clones did not compete more successfully than when confronting wildtype cells (Fig 3C-D). Importantly, loss of Fmi alone did not

induce competition, as in eye discs comprising initially equal populations of *fmi*$^{-/-}$ and wildtype cells the *fmi* mutant cells grew equally well as the wildtype cells (Fig 2 Suppl 1A-C).

If the requirement of Fmi is a general feature of cell competition, it should be observable in other tissues. We therefore assessed whether depleting Fmi in wing disc >>Myc winner clones would also reverse the competition outcome. We used hsp-Flp to generate twin spot clones expressing UAS-Myc, and as in eye discs, those clones behaved like super-competitors. Myc clones were on average 1.7 times larger than the homozygous RFP+ (hRFP) twin spots (Fig 2E). However, when >>Myc clones lacked Fmi, their ability to compete was severely impaired, producing much smaller clones, being on average half as large as their hRFP twin spots, and thus, like in eye discs, behaved as one would expect of losers when competing against wildtype cells (Fig. 2F-H). Interestingly, *fmi*^{E59} Myc clones were also highly fragmented in the wing disc, a phenomenon we did not observe in eye discs. As observed in eye discs, removing Fmi from the wildtype losers had no effect on the ability of >>Myc clones to compete (Fig 3G-H). Similarly, making clones mutant for *fmi* alone had no effect on their growth in wing discs (Fig 2 Suppl 1D-F).

In the setting of tumorigenesis, either tumor cells or wildtype cells may emerge as winners of cell competition. Tumors outcompete wildtype cells in the processes of invasion and metastasis, whereas transformed pre-malignant cells are often eliminated by wildtype cells through competition-dependent defense mechanisms such as EDAC (Kon et al., 2017; Kon & Fujita, 2021). We therefore further explored the potential requirement for Fmi in a system in which both outcomes occur at different times. In eye discs, cells lacking Scrib display a proto-oncogenic behavior, losing polarity and over-proliferating in the developing eye disc. However, as eye development progresses, they subsequently become losers, and are eliminated via JNK-mediated apoptosis during late third instar and pupal development so that they are virtually absent from the tissue before the fly ecloses (Brumby & Richardson, 2003).

Using the ey-Flp system to activate RNAi against *scrib* in eye discs, we confirmed that downregulation of *scrib* generated clones that perdure through larval development (Fig 3D-E,M) but were eliminated from the tissue by the end of pupal development and were not detected in the adult eye (Fig 3F-F'). Compared to control RFP clones, which represented around 40% of the eye cell population in early third instar larva (Fig 3A-B,M, Suppl 1A) and remained at roughly that proportion in the adult eye (Fig 3C-C'), *scrib* RNAi clones began to be eliminated at or before the time the morphogenetic furrow progresses (Fig 3E,M, Suppl 1B), and were almost completely absent in adult eyes (Fig 3F-F'). Their elimination left scars in the adult eye, likely because the structure of the eye is established with the passing of the morphogenetic furrow, and the compound eyes were smaller compared to wildtype eyes (Fig 3C,F)). Wildtype cells therefore behave as winners when confronted with *scrib* RNAi clones during late larval and pupal development.

We then evaluated the effect of removing Fmi from the wildtype winner clones in *scrib* cell competition. Loss of *fmi* in wildtype cells had little impact on the size of *scrib* RNAi clones in third instar larval discs (Fig 3G-H,M, Suppl 1C), but as development progressed, wildtype winner cells depleted of *fmi* lost their ability to compete with and eliminate *scrib* RNAi clones; the *scrib* RNAi clones survived during pupal development and indeed constituted the majority of the adult eye (Fig 3I-I'), showing a reversal in the competition outcome much as the outcome of >>Myc competition is reversed when the winners lack Fmi. The surviving *scrib* RNAi cells failed to differentiate, and instead produced large scars in the adult eye (Fig 3I-I'). We also observed considerable lethality in this population of flies, presumably due to the uncontrolled proliferation of *scrib* RNAi cells that could not be eliminated.

During >>Myc supercompetition, removing Fmi from the loser wildtype cells showed no effect in cell competition in eye and wing discs (Fig 2C,G). We therefore considered what might happen if *scrib* RNAi loser clones are made to lack Fmi. However, this situation is more complex than the >>Myc competition, since *scrib* RNAi clones have been previously documented to initially overproliferate, perhaps behaving as winners, before ultimately becoming losers (Brumby & Richardson, 2003). We were unable to quantify this early proliferation of *scrib* RNAi eye clones before they are eliminated by their wildtype neighbors, as the discs are too small for us to dissect and count. However, assuming that they are behaving as winners in early larval development, one might expect that removing Fmi from *scrib* RNAi clones would impair their ability to overproliferate early, such that by third instar, they would be smaller than *scrib* RNAi clones with intact Fmi. Indeed, this is what we observed (Fig 3J,K,M, Suppl 1D). While some portion of their smaller size relative to control clones is attributed to their elimination by wildtype winners as described above, the remainder may be a result of the loss of their ability to overproliferate earlier in larval development.

The small population of fmi^{E59} *scrib* RNAi clones remaining at third instar was almost completely eliminated by the end of larval development, such that the adult eyes were indistinguishable from wildtype eyes (Fig 3L-L'). We hypothesize that the lack of *fmi* in *scrib* clones hinders their ability to overproliferate in early larval stages, resulting in smaller clones that are quickly eliminated by their wildtype neighbors, allowing compensatory differentiation to generate a morphologically normal eye.

Loss of fmi triggers cell death and reduces proliferation in "would-be" winner clones

Our observations suggest that lack of *fmi* renders winner clones and tumors incapable of outcompeting the neighboring tissue in multiple cell competition scenarios. Cell competition relies mainly on two mechanisms to allow winner cells to take over the tissue when confronting less fit cells: faster proliferation than losers and elimination of loser cells by induced apoptosis or extrusion (Amoyel & Bach, 2014; Maruyama & Fujita, 2017; Morata, 2021). We therefore explored how the lack of *fmi* in tumors and winner >>Myc cells during competition affected both mechanisms.

Drosophila control Ras^{V12}, *scrib* RNAi eye tumors trigger apoptosis in the neighboring cells, as detected by Dcp1 staining (Fig 4A-D), consistent with previous reports (Karim & Rubin, 1998; Pérez et al., 2017) and with their highly invasive behavior when surrounded by wildtype cells. However, when *fmi* was removed from the clonal tumors, the outcome of this competition was reversed, as described above, and instead, $fmi^{-/-}$, Ras^{V12}, *scrib* RNAi tumors displayed excess apoptosis compared to the surrounding wildtype tissue (Fig 4E-H). Moreover, we found cell debris from *fmi*-deficient tumor cells inside lysosomal vesicles in wildtype cells, suggesting that wildtype cells are clearing neighboring loser tumor cells through engulfment (Fig 4 Suppl 1). We then tested whether this reversal of apoptosis burden was specific to the tumor model, or if it is a mechanism shared in other cell competition models. We counted apoptotic cells in WT and >>Myc clones in the eye disc only when these cells were located near to the clone boundary (1-3 cells from the boundary, see methods for details). We observed that control >>Myc clones showed low levels of apoptosis and similar levels in their neighboring WT cells (Fig. 4I-L; p-value 0.6049), in line with previous results (de la Cova et al., 2004), whereas, consistent with the tumor model, apoptosis was significantly increased in fmi^{E59}, >>Myc clones but not in their WT neighbors (Fig 4M-P, p-value 0.0006), likely contributing to the reversal in competition we previously observed (Fig 2A-D).

JNK signaling plays a prominent role during cell competition. Previous reports have shown that activation of JNK mediates engulfment and elimination of *scribble* clones during cell competition (Ohsawa et al., 2011; Yamamoto et al., 2017). However, JNK signaling is also responsible for increased tumor growth and invasion in Ras-activated cells or scrib mutants (Igaki et al., 2006; Uhlirova & Bohmann, 2006; Leong et al., 2009). We therefore asked whether the role of Fmi in tumorigenesis and cell competition could be related to the regulation of JNK signaling. Confirming previous observations, we detect activation of JNK signaling via the *puckered* lacZ reporter puc^{E69} both in Ras^{V12}, *scrib* RNAi tumors (Fig 4A-C), and *scrib* RNAi clones in eye discs (Fig 4 Suppl 2A-C). However, Ras^{V12} tumors lacking *fmi*, despite displaying cell death in tumor cells competing with wildtype neighbors, show no change in Puc activation (Fig 4E-G). Similarly, *scrib* RNAi clones activate JNK signaling independently of *fmi* (Fig 4 Suppl 2D-F). We therefore conclude that Fmi acts independently of JNK signaling.

Cell competition does not rely solely on apoptosis to eliminate loser cells. An increased proliferation rate of winners is also a hallmark of cell competition (Morata, 2021; Madan et al., 2022). To evaluate whether Fmi is also required to maintain a higher proliferative ratio in winners, we quantified mitotic cells in winner clones with and without Fmi. The wing disc displays distributed cell divisions throughout larval development, in contrast to eye discs, where passing of the morphogenetic furrow limits proliferation as cells start differentiating into compound eye cells (Wolff & Ready, 1991; Tsachaki & Sprecher, 2012). Therefore, for the quantification of proliferation, the wing is a better model than the eye disc. When wing disc >>Myc clones were depleted of Fmi, cell proliferation, as measured by pHis3 staining, was significantly reduced (Fig 4Q-S). Taken together, these observations directly link the need for Fmi to proliferation and induced apoptosis, the two key events of cell competition, in several models of cell competition.

Fmi mediated cell-cell communication is not required for competition between winners and losers

Previously, some key players involved in cell competition, including Flower (Rhiner et al., 2010) and Xrp-1 (Baillon et al., 2018), were shown to be either up- or down-regulated during competition. We evaluated whether Fmi protein levels might also be affected during competition. Fmi is ubiquitously expressed at low levels in *Drosophila* larva, pupa and adult (Brown et al., 2014). We stained third instar larval wing discs with >>Myc clones to determine whether >>Myc supercompetition affects the levels of Fmi protein at the membrane, either inside the clone or near the boundary where cell competition occurs. We observed no change in Fmi protein levels (Fig 5 Suppl 1), suggesting that Fmi is involved in competition through a mechanism that does not rely on altering protein levels.

Cell competition is thought to rely on intercellular communication to compare fitness and determine the outcome between prospective winner and loser cells (Kon et al., 2017; Baker, 2020; Ogawa et al., 2021). If Fmi is involved in these determinative intercellular communication events by signaling as a trans-homodimer, it should be required in both prospective winner and loser cells. Our previous eye and wing disc >>Myc supercompetition results already suggested this is not the case. While the removal of *fmi* caused winner clones to effectively become losers during >>Myc competition (Fig 2), removing *fmi* from the losers had no effect on the losers' outcome, either in eye discs (Fig 2C-D) or wing discs (Fig 2G-H). In both tissues, winner >>Myc clones showed no change in relative size to their twin spot counterparts, nor were loser clones eliminated more effectively (Fig 2D and 2H).

Our results so far suggested that the effect Fmi exerts on cell competition does not operate through bidirectional intercellular PCP communication. To further consolidate this hypothesis, we examined the effect of removing a dedicated core PCP protein other than Fmi from >>Myc supercompetitors. Generating *vang*^{A3} >>Myc clones in the wing disc, we observed that the >>Myc clones were unaffected and remained winners (Fig 5). *vang*^{A3}, >>Myc clones were on average 2.2±0.82 times larger than their hRFP twins, not significantly different from the 1.7±0.45 fold value for >>Myc clones (Fig 2H; Fig 5C).

The activity of Fmi in cell competition does not require its cadherin domains

Our results have so far demonstrated that Fmi is required only in winner cells and that its function in cell competition is independent of PCP. Furthermore, our results rule out a role for Fmi homodimers in directly communicating fitness information between prospective winner and loser cells. However, the possibility remained that Fmi might function through trans-homodimerization between prospective winner cells to sustain winner status via a signal, via adhesion, or both. To ask if Fmi fulfills its role by mediating adhesion, we tested whether we could restore winner status to >>Myc clones that lack Fmi by providing a transgenic *fmi* that lacks the 9 cadherin domains of Fmi (*arm-fmiΔCad*).

Coexpression of *arm-fmiΔCad* in *fmi*^{E59}, >>Myc clones re-established the ability of these clones to outcompete their neighbors, and they again became supercompetitors (Fig. 6). When comparing the ratio of >>Myc clone cell number to twin spot cell number, the presence of *arm-fmiΔcad* restores competition to a level comparable to >>Myc supercompetitors (1.43±0.48 GFP/hRFP cells vs 1.71±0.45 GFP/hRFP cells respectively), far above the 0.49±0.29 value for *fmi*^{E59} >>Myc clones compared to twin spots.

Supercompetitor clones mutant for *fmi* consistently show clone fragmentation (Figs. 2F, 4R, 6B). Despite lacking the cadherin repeats, rescued clones not only restored their supercompetitor status, but fully recovered the ability of >>Myc clones to remain cohesive (Fig. 6C). This suggests that the clone fragmentation we observed is unlikely due to the ability of Fmi to contribute to adhesion and more likely caused by a feature of the competition between wildtype cells and *fmi*$^{-/-}$ >>Myc loser clones that causes their elimination.

Taken together, these results demonstrate that, while Fmi is essential in winner cells to eliminate less fit neighbors, this effect is independent of PCP or other homodimer-mediated signaling, and independent of Fmi-mediated cell adhesion, suggesting instead an as yet uncharacterized function for Fmi.

Discussion

We have identified a requirement for Fmi in winner cells in both tumorigenic and developmental cell competition models. Cells that would otherwise behave as winners instead behave as losers when they lack Fmi. Fmi is notable in that it is required in cell competition in each of four distinct competition scenarios examined: Ras^{V12} *scrib* RNAi tumors, Myc supercompetitor clones in eye and wing discs, wildtype cells *vs scrib* RNAi loser clones in pupal eyes, and likely *scrib* RNAi clones in larval eye discs. Just how universal this requirement is in other cell competition scenarios in *Drosophila* and perhaps in competition in other organisms remains to be determined.

Fmi acts in cell competition independently of PCP

Several arguments support the conclusion that the role for Fmi in cell competition is distinct from its role in PCP signaling. First, Fmi is the only core PCP component among the six that were surveyed to inhibit the ability of Ras^{V12} *scrib* RNAi tumor clones to compete in the eye. If Fmi's role in cell competition were to signal winner fate to losers and vice versa by mirroring its role in PCP signaling, where it signals the presence of proximal (Vang, Pk) components in one direction and the presence of distal components (Fz, Dsh, Dgo) in the other direction between adjacent cells (Lawrence et al., 2004; Strutt & Strutt, 2007; Strutt & Strutt, 2008; Chen et al., 2008; Struhl et al., 2012), then one might expect either the proximal or distal components to also be required in winner clones. No such requirement was observed. Second, in PCP signaling, Fmi functions as a trans-homodimer to transmit those signals and requires the cadherin repeats and other extracellular domains, implying its function as a trans-homodimer (Kimura et al., 2006). In PCP signaling, removing Fmi from either of two adjacent cells completely blocks PCP signaling. In contrast, in cell competition, while Fmi is required in winners, removing Fmi from losers has no effect on competition. Thus, the model of bidirectional signaling via Fmi is not supported by our results.

These observations, however, do not rule out the possibility that Fmi trans-homodimers contribute to intercellular signaling among winner cells. Nonetheless, as discussed above, adhesion seems not to be a meaningful part of the function for Fmi in winners, as an adhesion deficient Fmi construct (*fmiΔCad*) fully rescues both competition and clone adhesion. The potential contributions of adhesion vs other possible signaling mechanisms are discussed at more length below.

Unlike the other core PCP genes, $fmi^{-/-}$ mutations are lethal due to requirements in the nervous system (Usui et al., 1999). Though not fully characterized, it's roles in the nervous system appear to be distinct from PCP signaling. Fmi is required for outgrowth and guidance of the R8 axon of the eye to the M3 layer of the medulla via a mechanism that appears independent of other components of the core PCP signaling pathway (Gao et al., 2000; Lee et al., 2003; Senti et al., 2003), but does interact with Golden goal, a transmembrane phosphoprotein that is not associated with PCP signaling (Takechi et al., 2021). Growth of the dendrites of dorsal da neurons is also regulated by Fmi. During embryogenesis, da dendrites in *fmi* mutant embryos emerge precociously and overgrow as they approach the dorsal midline, and later, during larval growth, dendrites from opposite sides fail to avoid each other (tile) and instead overlap (Gao et al., 2000; Sweeney et al., 2002; Kimura et al., 2006).

Fmi is classified as an atypical cadherin and a Class-B adhesion G Protein-Coupled Receptor (AGPCR), as it contains in its extracellular domain several conserved functional domains including cadherin repeats, epidermal growth factor-like repeats, laminin A G-type repeats, and a GPCR autoproteolytic inducing (GAIN) domain that contains within it a GPCR proteolytic site (GPS) (Rosa et al., 2021; Einspahr & Tilley, 2022; Sreepada et al., 2022). These extracellular domains are followed by seven transmembrane domains and an intracellular C-terminal domain. Although much remains to be learned about this large subfamily of GPCRs, a general model has emerged in which activation by membrane bound or extracellular protein, peptide, proteoglycan or small molecule ligand, or mechanical force exposes a tethered ligand at the N-terminus of the C-terminal fragment in the GAIN domain that, upon exposure, interacts with the transmembrane portion to activate a G-protein signaling cascade. In many but not all AGPCRs, the tethered ligand is exposed by GAIN domain-mediated autoprotolysis of its GPS. Non-cleaved AGPCRs are hypothesized to expose the tethered ligand by an allosteric conformational change. Some de-orphanized AGPCRs interact with multiple ligands, and ligand binding can result in partial or full

activation. In some cases, it appears that engineered truncation of portions of the extracellular domain can produce some level of ligand independent activation (Rosa et al., 2021).

When expressed in da neurons, a Fmi construct lacking the cadherin, laminin G and EGF-like repeats partially rescued the embryonic dendritic overgrowth phenotype (Kimura et al., 2006), suggesting a function independent of homodimerization. The G protein Gαq (Gq) has been proposed to function downstream of Fmi to mediate this repressive function (Wang et al., 2016). A recent preprint reports the resolved structure of the CELSR1 extracellular domain, showing that the protein has two distinct domains: an adhesion domain comprised of the first 8 Cadherin repeats, and a compact domain that extends from the ninth cadherin repeat to the transmembrane domains that is involved in GPCR signaling. Indeed, they demonstrated that a CELSR1 construct lacking only the Cadherin repeats 1-8 retains the ability to activate Gαs, which has been predicted to interact with CELSR1 (Bandekar et al., 2024). Notably, our results showed that a similar Fmi construct lacking the cadherin domains substantially rescues the requirement for Fmi in winner cells during cell competition (Fig. 6). These observations suggest that supplying adhesion is not the principal function of Fmi in these events, but are consistent with the possibility that homodimeric adhesion, or interaction with a different ligand, normally activates the receptor, and that the truncated FmiΔCad behaves as a constitutively activated receptor capable of binding to either Gα proteins. While no biochemical characterization of Fmi has been reported, the human orthologs CELSR1-3 have been studied in detail. CELSR2 is autoproteolytically cleaved while CELSRs 1 and 3 are not, yet all three couple to GαS (Huong Bui et al., 2023). Additional efforts will be required to determine the functional ligand(s) for Fmi and whether it signals similarly. Furthermore, AGPCRs participate in a wide variety of developmental and physiologic events through diverse effectors (Einspahr & Tilley, 2022; Sreepada et al., 2022). The pathway by which Fmi participates in cell competition remains to be explored.

Fmi, cell competition and cancer

When the first examples of super-competition were observed in Myc clones and the Hippo pathway (Moreno & Basler, 2004; de la Cova et al., 2004; Ziosi et al., 2010; Neto-Silva et al., 2010), they hinted at the possibility that tumors, which behave like super-competitors, could use similar mechanisms to outcompete wildtype cells. Understanding tumor competition may open new avenues for early detection and therapy (Baker & Li, 2008; Moreno, 2008).

Research in *Drosophila* and mammals has shown that cell competition plays a dual role during tumorigenesis. Cells harboring mutations in proto-oncogenes or tumor-suppressor genes often behave as losers (Maruyama & Fujita, 2017; Morata & Calleja, 2020; Kanda & Igaki, 2020). Through the process of EDAC, epithelial tissues use cell competition to eliminate transformed pre-neoplastic cells by removing them from the tissue via directed cell death or extrusion (Kon et al., 2017; Watanabe et al., 2018). Pre-neoplastic cells that escape EDAC may accumulate additional mutations to become malignant tumors (Watanabe et al., 2018). Malignant tumors not only escape EDAC, but acquire properties that allow them to outcompete wildtype cells, facilitating invasion and metastasis (Suijkerbuijk et al., 2016; Kohashi et al., 2021). Furthermore, competition between clones within tumors further selects for more aggressive tumor behavior (Parker et al., 2021).

Another commonality between developmental and oncogenic cell competition is the involvement of the transmembrane protein Flower (Fwe). In both *Drosophila* and mammals, multiple isoforms of Fwe signal fitness; expression of Fwe^{Lose} isoforms mark losers for elimination (Rhiner et al., 2010; Merino et al., 2013; Levayer et al., 2015; Madan et al., 2019). Forced expression of Fwe^{Lose} induces cell competition and elimination of the loser, suggesting that Fwe comparison is involved in the sensing and/or initiation of differential fitness. This contrasts with Fmi, whose differential expression does not act as a trigger for competition, but which is needed in winners to allow them to win, suggesting that Fmi is involved after sensing in the execution of functions necessary to manifest winner behavior.

Evidence is accumulating that a human ortholog of Fmi, CELSR3, is expressed at high levels in a range of solid tumors, including lung, prostate, pancreatic, hepatic, ovarian and colorectal cancers, and in some cases has been shown to be associated with poor prognosis (Katoh & Katoh, 2007; Erkan et al., 2010; Asad et al., 2014; Goryca et al., 2018; Li et al., 2021; Chen et al., 2021a)**.** Recently, CELSR1 upregulation has also been linked to poor ovarian cancer prognosis, likely by promoting proliferation, migration, and invasion (Zuo et al., 2023). If CELSR1/3 are promoting winner cell behavior in these tumors, as might be predicted from its function in *Drosophila*, this could provide the rationale for future efforts to understand the mechanism by which Fmi/CELSR3 facilitates cell competition, with the goal of identifying an intervention that could blunt or perhaps even eliminate the aggressiveness of an array of highly morbid cancers.

Acknowledgements

We would like to thank members of the Axelrod lab for fruitful discussions. Stocks obtained from the Bloomington Drosophila Stock Center (NIH P40OD018537) were used in this study.

This work was funded by NIH R35GM131914 (J.D.A.) and the Swiss National Science Foundation P400PB_199258 (P.S.B.). The funders had no role in study design, data collection and analysis, decision to publish, or preparation of the manuscript.

Conflict of interest

The authors declare that the research was conducted in the absence of any commercial or financial relationships that could be construed as a potential conflict of interest.

Figure legends

Figure 1. Fmi is required in clonal tumors to outcompete wildtype tissue.

A) Schematic of the whole eye disc Ras^{V12}, scrib RNAi, RFP tumors.

B-H) Pupal RFP tumors imaged through the cuticle. All pupae are ey-Flp ; act5C>CD2>Gal4, UAS-RFP with the indicated RNAi. N = 5 (no tumor), 10 (control RNAi), 13 (*fmi* RNAi), 17 (*fz* RNAi), 19 (*dsh* RNAi), 17 (*vang* RNAi) and 8 (*pk* RNAi).

C) Control UAS-Ras^{V12}, UAS-scrib RNAi, UAS-w RNAi tumors.

D-H) UAS-RasV12, UAS-scrib RNAi tumors co-expressing UAS-RNAi against the PCP genes indicated above each pupa.

B'-H') Representative third instar larval brain and eye discs for each of the experimental groups from above. Arrowheads in B' point to the eye-antenna imaginal disc (orange) and the brain lobes (green). N = 3 (no tumor), 10 (control RNAi), 13 (*fmi* RNAi), 12 (*fz* RNAi), 15 (*dsh* RNAi), 20 (*vang* RNAi) and 10 (*pk* RNAi).

I) Schematic of eye disc Ras^{V12}, scrib RNAi, RFP clonal tumors.

J-P) Third instar larval eye discs RFP tumor clones generated via ey-Flp ; FRT42D Gal80 / FRT42D ; act5C>CD2>Gal4, UAS-RFP.

J) Eye discs with non-tumor, control RFP clones.

K) Control Ras^{V12}, UAS-scrib RNAi, RFP clonal tumors.

L-P) Ras^{V12}, scrib RNAi, RFP clonal tumors carrying the PCP allele indicated above each panel.

Scalebars: 100 µm

Figure 2. Winners require Fmi in developmental supercompetition.

A) Eye imaginal disc clones overexpressing UAS-Myc (>>Myc) and UAS-nGFP under control of the tub>CD2>GAL4 driver. Clones were generated with ey-Flp, so half of the cells are clones and the other half are wildtype twins.

B) Eye imaginal disc >>Myc, UAS-nGFP, *fmi*^{E59} clones, competing against wildtype twins.

C) Eye imaginal disc >>Myc, UAS-nGFP clones, competing against *fmi*^{E59} twins.

D) Ratio of RFP-labeled clone area versus unlabeled wildtype area. The unlabeled wildtype area was obtained by subtracting the RFP-labeled area from the total eye disc area. A ratio over 1 implies RFP-positive clones are over-represented, likely behaving as supercompetitors, while a ratio below 1 means the RFP-cells are under-represented, likely losers. N = 9 discs (>>Myc), 5 discs (*fmi*^{E59}, >>Myc), 4 discs (*fmi*^{E59} vs >>Myc), groups were analyzed using multiple unpaired, two-tailed t test; p-values: <0.0001 (****), 0.6340 (ns)

E) Representative wing imaginal disc overexpressing >>Myc and UAS-nGFP under control of the tub-Gal4 driver. Clones were generated using hsp70-Flp, with a 15 min 37ºC heat-shock. wildtype cells are labeled with tub-nRFP. Non-recombinant cells are heterozygous for nRFP, while twin spots are homozygous nRFP. n = 14 discs

F) Representative wing imaginal disc with >>Myc, UAS-nGFP, *fmi*^{E59} clones, over a wildtype background. Clones were generated in the same fashion as D. n = 19 discs

G) Representative wing imaginal disc with >>Myc, UAS-nGFP clones, competing against *fmi*^{E59} twin spots. n = 13 discs

H) log10 of the >>Myc/Twin spot cell ratio. nGFP total cells were divided by the number of twin spot homozygous nRFP cells, and then log10-transformed. A ratio over 0 indicates over-representation (likely supercompetition) of nGFP+ clones, and below 0 indicates nGFP+ cells are under-represented (likely behaving as losers). The difference between groups was analyzed using a one way ANOVA, with Dunnett correction for multiple comparisons; p-value: >>Myc vs *fmi*^{E59} >>Myc < 0.0001 (****); >>Myc vs *fmi*^{E59} = 0.9705 (ns).

Scalebars: 50 µm

Figure 3. Winners require fmi in *scribble* cell competition

A-L') scrib RNAi clone analysis in the prospective eye. UAS-scrib RNAi was expressed with the act5C>CD2>Gal4 driver and clones were generated by ey-Flp. Clones are marked both with UAS-nGFP and tub-nRFP.

A) Representative early third instar disc with control UAS-nGFP clones.

B) Representative late third instar disc with control UAS-nGFP clones.

C-C') Representative adult eye with control UAS-nGFP clones. C' shows fluorescently labeled control clone cells.

D) Representative early third instar disc with UAS-scrib RNAi clones versus wildtype twin clones.

E) Representative late third instar disc with UAS-scrib RNAi clones versus wildtype twin clones.

F-F') Representative adult eye with UAS-scrib RNAi clones versus wildtype twin clones. F' shows fluorescently labeled surviving UAS-scrib RNAi cells.

G) Representative early third instar disc with UAS-scrib RNAi clones versus *fmi*^{E59} twin clones.

H) Representative late third instar disc with UAS-scrib RNAi clones versus *fmi*^{E59} twin clones.

I-I') Representative adult eye with UAS-scrib RNAi clones versus *fmi*^{E59} twin clones. This phenotype was lethal. The adult eye shown was from an escaper. Escapers had trouble eclosing and died within hours. I' shows fluorescently labeled surviving scrib RNAi cells. tub-nRFP fluorescence was barely visible, so the stronger UAS-nGFP is shown.

J) Representative early third instar disc with *fmi*^{E59}, UAS-scrib RNAi clones versus wildtype twin clones.

K) Representative late third instar disc with *fmi*^{E59}, UAS-scrib RNAi clones versus wildtype twin clones.

L-L') Representative adult eye with *fmi*^{E59}, UAS-scrib RNAi clones versus wildtype twin clones. L' shows fluorescently labeled surviving *fmi*^{E59}, UAS-scrib RNAi cells.

M) Quantification of fluorescently tagged clone area for the phenotypes mentioned above. Each dot in the violin plot displays the ratio of RFP+ area versus total disc area. Of special significance is the fact that scrib RNAi clones competing with wildtype clones survive similarly to scrib RNAi clones competing with *fmi*^{E59}. P-values are as follow: **** < 0.0001; *** < 0.0005; ns = 0.2634

Scalebars: 50 µm

Figure 4. Lack of Fmi increases cell death and reduces proliferation in would-be winners.

A-C) Ras^{V12}, scrib RNAi tumors stained for DAPI, Dcp1+ (A), and puc-lacZ (B). C) Merged channels

D) Representation of how Dcp1+ staining localizes in the wildtype cells at the boundary with the tumor.

E-G) Ras^{V12}, scrib RNAi tumors mutant for Fmi, stained with DAPI, Dcp1+ (E), and puc-LacZ (F). G) Merged channels.

H) Representation of how Dcp1+ staining localizes in the tumor cells in contact with the surrounding wildtype tissue.

Scalebar for A-G: 25 µm

I-K) Dcp1+ staining in >>Myc clones in eye discs. >>Myc clones are marked by GFP (I) and were stained against Dcp1+ (J). The arrows shows apoptotic WT (red arrow) and >>Myc (white arrow) cells at the clone boundary. K) Merged channels, showing apoptotic cells evenly distributed between WT and >>Myc cells.

L-N) Dcp1+ staining in >>Myc clones lacking Fmi in the eye disc. Eye disc >>Myc clones are marked by GFP (L) and were stained for Dcp1+ (M). N) Merged channels, showing apoptotic cells localized mainly in the >>Myc, fmi^{E59} clones.

Scalebar: 50 µm

O) Quantification of apoptotic cells in WT versus >>Myc clones in eye discs. Apoptosis occurs similarly in WT and >>Myc cells (two-tailed paired t-test; p-value = 0.6049). The left side of the graph shows the number of apoptotic WT and >>Myc cells. Each imaginal disc is displayed as a pair of dots, linked by a line, to easily visualize the Dcp1+ apoptotic cells in WT versus >Myc cells. Dots represent the number of apoptotic WT (left) or >>Myc (right) cells per disc. The right side of the graph displays the difference (>>Myc minus WT apoptotic cells). The dashed line indicates the mean difference between those values for all samples. N = 14 discs.

P) Quantification of apoptotic cells in WT versus >>Myc, fmi^{E59} clones in eye discs. Apoptosis is found mainly in >>Myc, fmi^{E59} cells (two-tailed paired t-test; p-value = 0.0006). The left side of the graph shows the number of apoptotic WT and >>Myc, fmi^{E59} cells, side by side. Dots represent the number of apoptotic >>WT (left) or >>Myc, fmi^{E59} (right) cells per disc.The right side of the graph displays the difference (>>Myc, fmi^{E59} minus WT apoptotic cells) . The dashed line indicates the mean difference between those values for all samples. N = 14 discs.

Q-R) Proliferation analysis performed by pHis3 staining in wing discs with either >>Myc clones (Q) or >>Myc, fmi^{E59} clones (R).

Scalebar: 20 µm

S) Proliferative ratio of GFP cells in a non-competition Control (n=9 discs), >>Myc (n=9 discs), or >>Myc, fmi^{E59} (n=13 discs) clones. The proliferative ratio for each group was calculated as the ratio of pHis3 cells within the GFP+ clone versus the non-GFP wildtype tissue and the differences were analyzed as an ordinary ANOVA with a Tukey's test for multiple comparisons, with all p-values < 0.0001 (****)

Figure 5 Vang is not required for >>Myc supercompetition

A) Representative wing imaginal disc showing the GFP-tagged, *vang*^{A3} >>Myc clones. Clones were generated using hsp70-Flp

B) RFP-labeled twin spots for the clones shown in A. Twin spot homozygous for RFP can be observed adjacent to the supercompetitor clones.

C) Graph showing the total GFP and homozygous RFP counts per disc, with each disc counts linked by a line and the log10 ratio of GFP/hRFP cells per disc (n=12 discs). Differences between GFP/hRFP clone size were analyzed using a two-tailed, ratio-paired t test. p-value<0.0001. When the ratio was compared with a two-tailed t test to >>Myc, the difference was not significant, with a p-value of 0.078.

Scalebar: 50 µm

Figure 6. The Fmi cadherin repeats are not required for cell competition.

A) Representative disc with nGFP-labeled, >>Myc (A), >>Myc, *fmi*^{E59} (B) or >>Myc, *fmi*^{E59}, *arm-fmiΔcad* (C) clones competing against wildtype twin spots in the wing disc. Twin spot clones are labeled with homozygous nRFP and clones were generated with hsp70-Flp.

D) Ratio of GFP versus RFP cells in the three groups, represented as the log10(GFP/hRFP) cell ratios. To evaluate the effect of the *arm-fmiΔcad* rescue (n=14 discs), the GFP/hRFP cell ratio was directly compared against the two other groups, already quantified and shown in Fig. 2F. Differences between the groups were analyzed using an unpaired, ordinary one-way ANOVA, which found a p-value <0.0001. Inter-group differences were analyzed with a Tukey multiple comparisons test, which found no differences between >>Myc and >>Myc, *fmi*^{E59}, *arm-fmiΔcad* clones, whereas both groups strongly differed from >>Myc, *fmi*^{E59} clones, both returning a p-value <0.0001 (****) when compared directly against >>Myc, *fmi*^{E59}.

Scalebar: 50 µm

Figure 1 Supplement 1. The ey-Flp recombination system causes almost every cell in the eye disc to undergo chromosomal recombination.

A) GFP-marked clonal cells. Clones generated with ey-Flp ; FRT42D tub-Gal^{80} / FRT42D tub-RFP ; ac>Gal4 UAS-GFP, express GFP in one of two daughter cells undergoing recombination to create homozygous clones without tub-Gal^{80}.

B) RFP-marked cells. Upon recombination, the same cells that express GFP also express two copies of tub-RFP, whereas cells that do not recombine express one copy of tub-RFP and lack GFP expression. We see few heterozygous RFP cells lacking GFP, indicating that few cells fail to undergo recombination in this system.

Figure 1 Supplement 2. *fmi* RNAi co-expression decreases the size of clonal Ras^{V12}, *scrib* RNAi tumors.

A) Ras^{V12}, *scrib* RNAi clonal tumors generated by ey-Flp co-expressing *w* RNAi, imaged in wandering third instar larvae. N = 5 larvae

B) Ras^{V12}, *scrib* RNAi clonal tumors generated by ey-Flp co-expressing *fmi* RNAi, imaged in wandering third instar larvae. N = 6 larvae

C) Ras^{V12}, *scrib* RNAi whole eye third instar larva tumor generated from ey-Flp clones, where the WT cells were eliminated using GMR-Hid, l(2)CL. N = 8 larvae

D) Ras^{V12}, *scrib* RNAi, fmi^{E59} whole eye tumor generated from ey-Flp clones, where the WT cells were eliminated using GMR-Hid, l(2)CL. N = 7 larvae

Scalebars: 200 µM

Figure 2 Supplement 1. Fmi by itself does not trigger cell competition

A) Eye disc GFP+ fmi^{E59} versus an unlabeled wildtype background. Clones were generated with ey-Flp as in Fig. 2A.

B) Eye disc GFP+, RFP control clones versus a wildtype background.

C) log of the GFP/WT clone ratio measured in either fmi^{E59} clones vs wildtype (n=11 discs) or RFP+ clones vs wildtype (n=15 discs). Differences were analyzed by a two-tailed, unpaired t test, rendering a p-value of 0.7655

D) Representative wing imaginal disc showing the GFP+ fmi^{E59} clone cells. Clones were generated with hsp70-Flp.

E) Twin spot RFP+ cells for the disc shown in D. Homozygous RFP+ twin spots can be observed adjacent to the RFP- fmi^{E59} clones.

F) fmi^{E59}, GFP cells versus wildtype homozygous RFP twin spot cells counted in wing imaginal discs (n=10 discs). The differences were analyzed with a two-tailed, ratio-paired t test, p-value = 0.4815

Scalebar: 50 µm

Figure 3 Supplement 1. Clone size during early third instar *scrib* competition

A) Percentage of RFP clone area in wildtype third instar discs. The X axes indicates the disc size measured as the total nuclear count in the eye imaginal disc. The line represents the best linear fit to the samples plotted.

B) Percentage of RFP, *scrib* RNAi clone area competing with wildtype twins in third instar discs.

C) Percentage of RFP, *scrib* RNAi clone area competing with *fmiE59* twins in third instar discs.

D) Percentage of RFP, fmi^{E59}, *scrib* RNAi clone area competing with wildtype twins in third instar discs.

Figure 4 Supplement 1. Fmi-/- tumor cell debris is found in vesicles inside wildtype cells

A) Close-up of RFP-tagged *fmi*^{E59} RasV12, scrib RNAi tumors competing against unlabeled wildtype cells in eye discs. RFP+ tumor cells can be observed at the periphery, and RFP+ debris is detected in the unlabeled wildtype cells inside the annotated area.

B) Lysotracker staining marking acidic vesicles. Large, stained vesicles can be observed in the annotated area.

C) The merged channels show colocalization of the RFP+ cell debris with the lysosomal vesicles inside wildtype cells.

D) Closeup of the annotated region in panels A-C.

Scale bar: 25 µm

Figure 4 Supplement 2. Lack of fmi does not affect the activation of JNK signaling.

A-C) Closeup of late third instar eye discs showing *scrib* RNAi clones marked with RFP (A), *puckered* transcriptional activation using the puc-LacZ reporter (B) and a merge image showing both channels (C)

D-F) Closeup of late third instar eye discs showing *scrib* RNAi, fmi^{E59} clones marked with RFP (D), *puckered* transcriptional activation (E) and a merge image showing both channles (F).

Figure 5 Supplement 1. Fmi levels are not affected by cell competition.

A/D) Overview of representative imaginal discs with >>Myc clones labeled with nGFP (green) and Fmi immunostaining (white), obtained from different larvae.

B) >>Myc clone (green), from the annotated box shown in (A). The clone boundary is delimited with a dashed line.

C) Fmi staining (white) from the annotated box shown in (A). The clone boundary is delimited with a dashed line.

E) >>Myc clone (green), from the annotated box shown in (D). The clone boundary is delimited with a dashed line.

F) Fmi staining (white) from the annotated box shown in (D). The clone boundary is delimited with a dashed line.

Scalebars: 50 µm

Material and methods

RESOURCE AVAILABILITY

Lead contact

Further information and requests for resources and reagents should be directed to and will be fulfilled by the lead contact (jaxelrod@stanford.edu).

Materials availability

Plasmid and fly lines generated in this study are available from the lead contact upon request.

Data and code availability

Any additional information required to reanalyze the data reported in this paper is available from the lead contact upon request.

EXPERIMENTAL MODEL AND STUDY PARTICIPANT DETAILS

Fly stocks and husbandry

Flies were maintained in standard fly food in a temperature-controlled incubator at either 25ºC or 18ºC. Egg collections were performed over a timespan of 24 or 48 hrs. Vials with eggs were kept at 25ºC until heat-shocked for clone generation or dissected.

Heat-shock was performed for 15 min on late first instar and early second instar larvae, 48 hrs after egg laying (AEL). Vials were kept at 25ºC after heat-shock until larvae were dissected.

The following fly lines were used for the experiments:

- y, w, hsp-Flp act5C-Gal4, UAS-nGFP to generate wing disc clones.
- ey-Flp ; if /SM5^ ; TM2 / ^TM6b to generate eye disc clones and whole tumors.
- Bloomington TRiP UAS-RNAi lines RRID:BDSC_33623 (*w* control), RRID:BDSC_26022 (*fmi*), RRID:BDSC_31311 (*fz*), RRID:BDSC_31306 (*dsh*), RRID:BDSC_34354 (*vang*), RRID:BDSC_32413 (*pk*), RRID:BDSC_39073 (*scrib*).
- PCP mutant alleles FRT42D, fmi^{E45} / CyO, FRT42D, fmi^{E59} / CyO, FRT2A, fz^{R52} / TM6b, FRT42D, $vang^{A3}$, FRT42D dgo^{380}, FRT42D $pk^{pk\text{-}sple13}$.
- UAS-scrib RNAi ; act5C>CD2>Gal4, UAS-RFP, UAS-Ras^{V12} / TM6b to make whole eye tumors.
- UAS-scrib RNAi FRT42D, tub-Gal^{80} ; act5C>CD2>Gal4, UAS-RFP, UAS-Ras^{V12} / TM6b to generate tumor clones.
- UAS-scrib RNAi, FRT42D, tub-nRFP / FRT42D tub-Gal^{80} to generate scrib RNAi eye disc clones.
- FRT42D fmi^{E59} / FRT42D, tub-nRFP, tub-Gal^{80} to generate wing disc twin spots.
- UAS-dMyc / TM6b for eye and wing disc supercompetitor clones.
- FRT42D fmi^{E59}, arm-fmiΔCad to rescue wing disc clones.

Genotypes of experimental models

Figure 1

(B) ey-Flp ; act5C>CD2>Gal4, UAS-nRFP / TM6b

(C-H) ey-Flp ; UAS-scrib RNAi / UAS-DCR2 ; act5C>CD2>Gal4, UAS-nRFP, UAS-Ras^{V12} / TM6b crossed to the homozygous UAS-RNAi line noted above.

(J) ey-Flp ; FRT42D tub-Gal^{80} / FRT42D ; act5C>CD2>Gal4, UAS-nRFP / TM6b

(K) ey-Flp ; FRT42D tub-Gal^{80} / FRT42D ; act5C>CD2>Gal4, UAS-nRFP UAS-Ras^{V12} / UAS-*scrib* RNAi

(L) ey-Flp ; FRT42D tub-Gal^{80} / FRT42D *fmi*^{E45} ; act5C>CD2>Gal4, UAS-nRFP UAS-Ras^{V12} / UAS-*scrib* RNAi

(M) ey-Flp ; act5C>CD2>Gal4, UAS-nRFP UAS-Ras^{V12} / UAS-*scrib* RNAi ; *fz*^{R52} FRT2A / tub-Gal^{80} FRT2A

(N) ey-Flp ; FRT42D tub-Gal^{80} / FRT42D *dgo*^{380} ; act5C>CD2>Gal4, UAS-nRFP UAS-Ras^{V12} / UAS-*scrib* RNAi

(O) ey-Flp ; FRT42D tub-Gal^{80} / FRT42D *pk*$^{pk\text{-}sple13}$; act5C>CD2>Gal4, UAS-nRFP UAS-Ras^{V12} / UAS-*scrib* RNAi

(P) ey-Flp ; FRT42D tub-Gal^{80} / FRT42D *vang*^{A3} ; act5C>CD2>Gal4, UAS-nRFP UAS-Ras^{V12} / UAS-*scrib* RNAi

Figure 2

(A) ey-Flp ; FRT42D tub-Gal^{80} / FRT42D; act5C>CD2>Gal4 UAS-nRFP / UAS-dMyc

(B) ey-Flp ; FRT42D tub-Gal^{80} / FRT42D *fmi*^{E59}; act5C>CD2>Gal4 UAS-nRFP / UAS-dMyc

(C) ey-Flp ; FRT42D *fmi*^{E59} tub-Gal^{80} / FRT42D tub-nRFP ; act5C>CD2>Gal4 UAS-nGFP / UAS-dMyc

(E) hsp-Flp tub-Gal4, UAS-nGFP ; FRT42D tub-nRFP tub-Gal^{80} / FRT42D ; UAS-dMyc / +

(F) hsp-Flp tub-Gal4, UAS-nGFP ; FRT42D tub-nRFP tub-Gal^{80} / FRT42D *fmi*^{E59} ; UAS-dMyc / +

(G) hsp-Flp tub-Gal4, UAS-nGFP ; FRT42D *fmi*^{E59} tub-nRFP tub-Gal^{80} / FRT42D ; UAS-dMyc / +

Figure 3

(A-C) ey-Flp ; FRT42D tub-Gal80 / FRT42D ; act5C>CD2>Gal4 UAS-nRFP / +

(D-F) ey-Flp ; FRT42D tub-Gal80 / FRT42D ; act5C>CD2>Gal4 UAS-nRFP / UAS-*scrib* RNAi *puc*^{E69}

(G-I) ey-Flp ; FRT42D tub-Gal80 / FRT42D *fmi*^{E59} ; act5C>CD2>Gal4 UAS-nRFP / UAS-*scrib* RNAi *puc*^{E69}

(J-K) ey-Flp ; FRT42D *fmi*^{E59} tub-Gal80 / FRT42D ; act5C>CD2>Gal4 UAS-nRFP / UAS-*scrib* RNAi *puc*^{E69}

Figure 4

(A-C) ey-Flp ; UAS-*scrib* RNAi FRT42D tub-Gal^{80} / FRT42D ; act5C>CD2>Gal4, UAS-nRFP UAS-Ras^{V12} / *puc*^{E69}

(E-G) ey-Flp ; UAS-*scrib* RNAi FRT42D tub-Gal^{80} / FRT42D *fmi*^{E59} ; act5C>CD2>Gal4, UAS-nRFP UAS-Ras^{V12} / *puc*^{E69}

(I-K) ey-Flp ; FRT42D tub-Gal^{80} / FRT42D *fmi*^{E59}; act5C>CD2>Gal4 UAS-nRFP / UAS-dMyc

(L) hsp-Flp tub-Gal4, UAS-nGFP ; FRT42D tub-nRFP tub-Gal^{80} / FRT42D ; UAS-dMyc / +

(M) hsp-Flp tub-Gal4, UAS-nGFP ; FRT42D tub-nRFP tub-Gal^{80} / FRT42D *fmi*^{E59} ; UAS-dMyc / +

Figure 5

(A-B) hsp-Flp tub-Gal4, UAS-nGFP ; FRT42D tub-nRFP tub-Gal^{80} / FRT42D *vang*^{A3} ; UAS-dMyc / +

Figure 6

(A) hsp-Flp tub-Gal4, UAS-nGFP ; FRT42D tub-nRFP tub-Gal^{80} / FRT42D ; UAS-dMyc / +

(B) hsp-Flp tub-Gal4, UAS-nGFP ; FRT42D tub-nRFP tub-Gal^{80} / FRT42D *fmi^{E59}* ; UAS-dMyc / +

(C) hsp-Flp tub-Gal4, UAS-nGFP ; FRT42D tub-nRFP tub-Gal^{80} / FRT42D *fmi^{E59}* arm-*fmiΔCad* ; UAS-dMyc / +

Figure 1 Supplement 1

(A-B) ey-Flp ; FRT42D tub-Gal^{80} / FRT42D tub-nRFP ; act5C>CD2>Gal4 / UAS-nGFP

Figure 1 Supplement 2

A) ey-Flp ; *scrib* RNAi FRT42D tub-Gal^{80} / FRT42D ; act5C>CD2>Gal4, UAS-nRFP, UAS-Ras^{V12} / *w* RNAi

B) ey-Flp ; *scrib* RNAi FRT42D tub-Gal^{80} / FRT42D ; act5C>CD2>Gal4, UAS-nRFP, UAS-Ras^{V12} / *fmi* RNAi

C) ey-Flp ; FRT42D / FRT42D GMR-Hid, l(2)CL-R ; act5C>CD2>Gal4, UAS-nRFP, UAS-Ras^{V12} / *scrib* RNAi

D) ey-Flp ; FRT42D *fmi^{E59}* / FRT42D GMR-Hid, l(2)CL-R ; act5C>CD2>Gal4, UAS-nRFP, UAS-Ras^{V12} / *scrib* RNAi

Figure 2 Supplement 1

(A) ey-Flp ; FRT42D tub-Gal^{80} / FRT42D ; act5C>CD2>Gal4 / UAS-nRFP

(B) ey-Flp ; FRT42D tub-Gal^{80} / FRT42D *fmi^{E59}* ; act5C>CD2>Gal4 / UAS-nRFP

(D-E) hsp-Flp tub-Gal4, UAS-nGFP ; FRT42D tub-nRFP tub-Gal^{80} / FRT42D *fmi^{E59}* ; MKRS / TM6b

Figure 4 Supplement 1

(A-C) ey-Flp ; FRT42D tub-Gal^{80} / FRT42D *fmi^{E45}* ; act5C>CD2>Gal4, UAS-nRFP UAS-Ras^{V12} / UAS-*scrib* RNAi

Figure 4 Supplement 2

(A-C) ey-Flp ; UAS-*scrib* RNAi FRT42D tub-Gal^{80} / FRT42D ; act5C>CD2>Gal4, UAS-nRFP UAS-Ras^{V12} / *puc^{E69}*

(D-F) ey-Flp ; UAS-*scrib* RNAi FRT42D tub-Gal^{80} / FRT42D *fmi^{E59}* ; act5C>CD2>Gal4, UAS-nRFP UAS-Ras^{V12} / *puc^{E69}*

Figure 5 Supplement 1

(A-F) hsp-Flp, tub-Gal4, UAS-nGFP ; FRT42D tub-Gal^{80} / FRT42D ; UAS-dMyc / +

METHOD DETAILS

Generation of arm-fmiΔCad

To make the *arm-fmiΔCad* construct, we used cDNA from the *fmi isoform A (stan-RA)* terminally tagged with an HA tag, fused using a SGGGGS linker (*fmi::HA*). We subcloned by Gibson assembly a PCR fragment containing the coding sequence for *fmi::HA* lacking the first 1328 aa, which contain the 9 cadherin domains (fmi$^{\Delta 1\text{-}1328}$) into a pCaSpeR4 vector backbone with the *armadillo* promoter and a Fz 5'UTR. The pCaSpeR4-armP-*fmiΔCad* construct was introduced into flies by P-element integration, and we used a fly line carrying the construct on chromosome arm 2R.

Wing imaginal disc dissection and immunohistochemistry

Third instar wandering larvae (120 hrs AEL) were dissected by transversally cutting the larva in two halves. The posterior half was discarded, and the anterior part was inverted, after which the fat body and digestive tissue (mouth hooks, salivary glands, and gut) were removed. Inverted larvae were fixed in 4% Paraformaldehyde (PFA) in phosphate buffered saline (PBS) + 0.02% Triton X-100 (PBS-T) for 30 min at room temperature (RT). Fixed larvae were then washed three times with PBS-T and then stained.

For antibody staining, larvae were stained with primary antibodies diluted in PBS-T + 3% Normal Donkey Serum (NDS) overnight (o/n) at 4ºC, and then stained with secondary antibodies and DAPI for 1 hr at room temperature. Stained larvae were then washed three times with PBS. Wing discs were carefully removed from the inverted larva and mounted in Vectashield mounting medium (Vector labs).

We used the following primary antibodies: rabbit α-pHis3 (Millipore), 1:100; rabbit α-Dcp1 (Cell Signaling), 1:100, Secondary staining was performed with Thermo Scientific 546-goat α-rabbit, 1:500.

Immunohistochemistry of third instar larval eye discs

Discs dissected from late third instar larvae were fixed for 5–15 min in 4% paraformaldehyde in PBS at 4°C. Fixed eye discs were washed two times in PBS-T. After blocking for 1 hr in 5% Bovine serum Albumin (BSA) in PBS-T at 4°C, discs were incubated with primary antibodies in the blocking solution overnight at 4°C. Incubations with secondary antibodies were done for 90 min at room temperature in PBS-T. Secondary antibody was washed 3 times with PBS-T. Incubations in phalloidin (1:200) and DAPI (1ug/mL), if required, were done in PBS-T for 15 min followed by washing at room temperature before mounting. Stained samples were mounted in 15 µl Vectashield mounting medium (Vector Labs). We used the following primary antibodies: mouse anti-LacZ (1:500 dilution, Promega) rabbit α-Dcp1 (1:500 dilution, Cell Signaling), mouse α-Fmi (1:200 dilution, DSHB). We used the following secondary antibodies from Thermo Scientific: 488-goat α-rabbit, 546-goat α-mouse, 594-donkey α-mouse, 647-donkey α-mouse. Alexa 635- and Alexa 350-conjugated phalloidin.

Image acquisition

Images of whole discs were taken with a Leica SP8 system equipped with a White Light Laser and HyD® detectors. A 40x, NA 1.5 Leica objective and 1.51 refractive index immersion oil were used. Image stacks were taken in 8-bit at 1024x1024 px resolution, and a pinhole of 1 airy unit (AU), using a z-step of 0.3 µM. For automated image quantification pipelines, residual tissue from the leg or haltere discs was removed in Fiji (fiji.sc, (Schindelin et al., 2012)), as well as the peripodial cells at the apical section of the Z-stack.

Adult eyes and RFP/GFP signal from pupae and eye discs isolated from late third instar larvae were imaged on a Leica MZ16F Stereomicroscope.

QUANTIFICATION AND STATISTICAL ANALYSIS

1. Eye disc clone analysis

Eye imaginal discs representative slices were selected to measure the size of RFP+ clones. To do so, the GFP+ clone area was divided by the non-fluorescent eye disc area to obtain the ratio of GFP+ clone vs non-GFP twin and plotted as the log10(ratio) on violin plots including all data points, median and

quartiles. Statistical analysis was performed in GraphPad Prism 10. Data was analyzed using unpaired, two-tailed t-tests.

2. Wing disc clone analysis

Wing imaginal disc GFP clone and RFP twin spot cell counts were obtained using a set of automated macros written for ImageJ (Sanchez Bosch & Axelrod, 2024). Cell ratios were obtained as the fraction of GFP+ cells vs RFP+ twin spot cells. Cell ratios were transformed as the log10(ratio) and graphed as violin plots including all datapoints, median and quartiles. Statistical analysis was performed in GraphPad Prism 10. Data was analyzed using either unpaired, two-tailed t-test (Fig 5), or an ordinary one-way ANOVA with a Tukey's multiple comparisons test (Figs 2, 3, 4 and 6).

3. Apoptosis quantification

Apoptotic cells marked with positive Dcp1 staining were scored when located 1-3 cells away from a clone boundary, as those were arbitrarily deemed as caused by cell competition. Cell counts were plotted individually, with each disc's WT and GFP cells plotted side-by-side, linked by a straight line. The difference in apoptosis between WT and >>Myc (or >>Myc, *fmi*^{E59}), GFP+ cells in each disc was then calculated (GFP minus WT cells) and plotted on the right. The mean difference of the analysis was also plotted in the same graph as a dashed line. The statistical differences were obtained using a paired, two-tailed t-test.

4. Cell proliferation quantification

Clone proliferation ratios were measured in ImageJ. First, we obtained the number of GFP+ cells versus the cells outside the GFP+ clones by using the same macros used to quantify GFP clones and then counting the total cells in the disc by counting the DAPI nuclei (Sanchez Bosch & Axelrod, 2024), and then subtracting the GFP+ cells from the total DAPI cell counts. Then, pHis3 positive cells were located by using the 3D Find maxima function from the ImageJ 3D Suite (https://mcib3d.frama.io/3d-suite-imagej/). To do so, the pHis3 channel was processed as follows: 1) specks were removed by using the Remove Outliers (radius of 5, threshold of 50), then the background was removed with a 2px 3D Gaussian Blur and the Subtract background function (rolling ball radius = 10 px, with sliding parabolic and disabled smoothing). Last, the pHis3+ peaks were found using the 3D Maxima finder (minimum threshold of 5 px, with a XY and Z radius of 3 px and discarding all peaks below the noise level of 20).

GFP+, pHis3 cells were obtained by first creating a binary mask of the GFP channel by smoothing the image with a 5 px 3D Gaussian blur and then using a Li threshold to create the mask. To ensure proper quantification, correct thresholding of the clones was visually assessed and adjusted when needed. Then, all pHis3 peaks that were inside the GFP+ clone were counted as proliferative GFP+ cells. Last the proliferative ratio of GFP+ cells was obtained by dividing the fraction of pHis3 cells inside GFP clones by the fraction of pHis3 cells outside of GFP+ clones. The log10 of the proliferative ratio was plotted as a violin plot representing each disc as a data point and indicating the median and quartiles. Statistical analysis was performed in GraphPad Prism 10. Data was analyzed using an ordinary one-way ANOVA and the groups were compared to each other using a Tukey's multiple comparisons test.

References

Adler, P. N. (2002). Planar signaling and morphogenesis in Drosophila. *Developmental Cell*, *2*(5), 525-535. http://eutils.ncbi.nlm.nih.gov/entrez/eutils/elink.fcgi?dbfrom=pubmed&id=12015961&retmode=ref&cmd=prlinks

Amoyel, M., & Bach, E. A. (2014). Cell competition: how to eliminate your neighbours. *Development*, *141*(5), 988-1000. https://doi.org/10.1242/dev.079129

Asad, M., Wong, M. K., Tan, T. Z., Choolani, M., Low, J., Mori, S., Virshup, D., Thiery, J. P., & Huang, R. Y. (2014). FZD7 drives in vitro aggressiveness in Stem-A subtype of ovarian cancer via regulation of non-canonical Wnt/PCP pathway. *Cell Death Dis*, *5*(7), e1346. https://doi.org/10.1038/cddis.2014.302

Baillon, L., Germani, F., Rockel, C., Hilchenbach, J., & Basler, K. (2018). Xrp1 is a transcription factor required for cell competition-driven elimination of loser cells. *Sci Rep*, *8*(1), 17712. https://doi.org/10.1038/s41598-018-36277-4

Baker, N. E., & Li, W. (2008). Cell competition and its possible relation to cancer. *Cancer Res*, *68*(14), 5505-5507. https://doi.org/10.1158/0008-5472.CAN-07-6348

Baker, N. E. (2020). Emerging mechanisms of cell competition. *Nature Reviews Genetics*, *21*(11), 683-697. https://doi.org/10.1038/s41576-020-0262-8

Bandekar, S. J., Garbett, K., Kordon, S. P., Dintzner, E., Shearer, T., Sando, R. C., & Araç, D. (2024). Structure of the extracellular region of the adhesion GPCR CELSR1 reveals a compact module which regulates G protein-coupling. *bioRxiv*, 2024.01.26.577439. https://doi.org/10.1101/2024.01.26.577439

Brown, J. B., Boley, N., Eisman, R., May, G. E., Stoiber, M. H., Duff, M. O., Booth, B. W., Wen, J., Park, S., Suzuki, A. M., Wan, K. H., Yu, C., Zhang, D., Carlson, J. W., Cherbas, L., Eads, B. D., Miller, D., Mockaitis, K., Roberts, J., Davis, C. A., Frise, E., Hammonds, A. S., Olson, S., Shenker, S., Sturgill, D., Samsonova, A. A., Weiszmann, R., Robinson, G., Hernandez, J., Andrews, J., Bickel, P. J., Carninci, P., Cherbas, P., Gingeras, T. R., Hoskins, R. A., Kaufman, T. C., Lai, E. C., Oliver, B., Perrimon, N., Graveley, B. R., & Celniker, S. E. (2014). Diversity and dynamics of the Drosophila transcriptome. *Nature*, *512*(7515), 393-399. https://doi.org/10.1038/nature12962

Brumby, A. M., & Richardson, H. E. (2003). scribble mutants cooperate with oncogenic Ras or Notch to cause neoplastic overgrowth in Drosophila. *EMBO J*, *22*(21), 5769-5779. https://doi.org/10.1093/emboj/cdg548

Butler, M. T., & Wallingford, J. B. (2017). Planar cell polarity in development and disease. *Nat Rev Mol Cell Biol*, *18*(6), 375-388. https://doi.org/10.1038/nrm.2017.11

Chen, W. S., Antic, D., Matis, M., Logan, C. Y., Povelones, M., Anderson, G. A., Nusse, R., & Axelrod, J. D. (2008). Asymmetric homotypic interactions of the atypical cadherin flamingo mediate intercellular polarity signaling. *Cell*, *133*(6), 1093-1105. https://doi.org/10.1016/j.cell.2008.04.048

Chen, X., Ma, Q., Liu, Y., Li, H., Liu, Z., Zhang, Z., Niu, Y., & Shang, Z. (2021a). Increased expression of CELSR3 indicates a poor prognostic factor for Prostate Cancer. *J Cancer*, *12*(4), 1115-1124. https://doi.org/10.7150/jca.49567

Chen, Y., Chen, Z., Tang, Y., & Xiao, Q. (2021b). The involvement of noncanonical Wnt signaling in cancers. *Biomed Pharmacother*, *133*, 110946. https://doi.org/10.1016/j.biopha.2020.110946

Chen, Z. S., Lin, X., Chan, T. F., & Chan, H. Y. E. (2021c). Pan-cancer investigation reveals mechanistic insights of planar cell polarity gene Fuz in carcinogenesis. *Aging (Albany NY)*, *13*(5), 7259-7283. https://doi.org/10.18632/aging.202582

Clavería, C., Giovinazzo, G., Sierra, R., & Torres, M. (2013). Myc-driven endogenous cell competition in the early mammalian embryo. *Nature*, *500*(7460), 39-44. https://doi.org/10.1038/nature12389

Coyle, R. C., Latimer, A., & Jessen, J. R. (2008). Membrane-type 1 matrix metalloproteinase regulates cell migration during zebrafish gastrulation: evidence for an interaction with non-canonical Wnt signaling. *Exp Cell Res*, *314*(10), 2150-2162. https://doi.org/10.1016/j.yexcr.2008.03.010

de la Cova, C., Abril, M., Bellosta, P., Gallant, P., & Johnston, L. A. (2004). Drosophila myc regulates organ size by inducing cell competition. *Cell*, *117*(1), 107-116. https://doi.org/10.1016/s0092-8674(04)00214-4

de Vreede, G., Gerlach, S. U., & Bilder, D. (2022). Epithelial monitoring through ligand-receptor segregation ensures malignant cell elimination. *Science*, *376*(6590), 297-301. https://doi.org/10.1126/science.abl4213

Di Giacomo, S., Sollazzo, M., Paglia, S., & Grifoni, D. (2017). MYC, Cell Competition, and Cell Death in Cancer: The Inseparable Triad. *Genes (Basel)*, *8*(4), 120. https://doi.org/10.3390/genes8040120

Einspahr, J. M., & Tilley, D. G. (2022). Pathophysiological impact of the adhesion G protein-coupled receptor family. *Am J Physiol Cell Physiol*, *323*(2), C640-C647. https://doi.org/10.1152/ajpcell.00445.2021

Ellis, S. J., Gomez, N. C., Levorse, J., Mertz, A. F., Ge, Y., & Fuchs, E. (2019). Distinct modes of cell competition shape mammalian tissue morphogenesis. *Nature*, *569*(7757), 497-502. https://doi.org/10.1038/s41586-019-1199-y

Erkan, M., Weis, N., Pan, Z., Schwager, C., Samkharadze, T., Jiang, X., Wirkner, U., Giese, N. A., Ansorge, W., Debus, J., Huber, P. E., Friess, H., Abdollahi, A., & Kleeff, J. (2010). Organ-, inflammation- and cancer specific transcriptional fingerprints of pancreatic and hepatic stellate cells. *Mol Cancer*, *9*, 88. https://doi.org/10.1186/1476-4598-9-88

Froldi, F., Ziosi, M., Garoia, F., Pession, A., Grzeschik, N. A., Bellosta, P., Strand, D., Richardson, H. E., Pession, A., & Grifoni, D. (2010). The lethal giant larvae tumour suppressor mutation requires dMyc oncoprotein to promote clonal malignancy. *BMC Biol*, *8*, 33. https://doi.org/10.1186/1741-7007-8-33

Gao, F. B., Kohwi, M., Brenman, J. E., Jan, L. Y., & Jan, Y. N. (2000). Control of dendritic field formation in Drosophila: the roles of flamingo and competition between homologous neurons. *Neuron*, *28*(1), 91-101. https://doi.org/10.1016/s0896-6273(00)00088-x

Goryca, K., Kulecka, M., Paziewska, A., Dabrowska, M., Grzelak, M., Skrzypczak, M., Ginalski, K., Mroz, A., Rutkowski, A., Paczkowska, K., Mikula, M., & Ostrowski, J. (2018). Exome scale map of genetic alterations promoting metastasis in colorectal cancer. *BMC Genet*, *19*(1), 85. https://doi.org/10.1186/s12863-018-0673-0

Gujral, T. S., Chan, M., Peshkin, L., Sorger, P. K., Kirschner, M. W., & MacBeath, G. (2014). A noncanonical Frizzled2 pathway regulates epithelial-mesenchymal transition and metastasis. *Cell*, *159*(4), 844-856. https://doi.org/10.1016/j.cell.2014.10.032

Hariharan, I. K., & Bilder, D. (2006). Regulation of imaginal disc growth by tumor-suppressor genes in Drosophila. *Annu Rev Genet*, *40*, 335-361. https://doi.org/10.1146/annurev.genet.39.073003.100738

Hogan, C., Dupré-Crochet, S., Norman, M., Kajita, M., Zimmermann, C., Pelling, A. E., Piddini, E., Baena-López, L. A., Vincent, J. P., Itoh, Y., Hosoya, H., Pichaud, F., & Fujita, Y. (2009). Characterization of the interface between normal and transformed epithelial cells. *Nat Cell Biol*, *11*(4), 460-467. https://doi.org/10.1038/ncb1853

Huong Bui, D. L., Roach, A., Li, J., Bandekar, S. J., Orput, E., Raghavan, R., Araç, D., & Sando, R. (2023). The adhesion GPCRs CELSR1-3 and LPHN3 engage G proteins via distinct activation mechanisms. *bioRxiv*, 2023.04.02.535287. https://doi.org/10.1101/2023.04.02.535287

Igaki, T., Pagliarini, R. A., & Xu, T. (2006). Loss of Cell Polarity Drives Tumor Growth and Invasion through JNK Activation in Drosophila. *Current Biology*, *16*(11), 1139-1146. https://doi.org/10.1016/j.cub.2006.04.042

Ji, Z., Chuen, J., Kiparaki, M., & Baker, N. (2021). Cell competition removes segmental aneuploid cells from Drosophila imaginal disc-derived tissues based on ribosomal protein gene dose. *Elife*, *10*, e61172. https://doi.org/10.7554/eLife.61172

Kanda, H., & Igaki, T. (2020). Mechanism of tumor-suppressive cell competition in flies. *Cancer Sci*, *111*(10), 3409-3415. https://doi.org/10.1111/cas.14575

Karim, F. D., & Rubin, G. M. (1998). Ectopic expression of activated Ras1 induces hyperplastic growth and increased cell death in Drosophila imaginal tissues. *Development*, *125*(1), 1-9. https://doi.org/10.1242/dev.125.1.1

Katoh, M. (2005). WNT/PCP signaling pathway and human cancer (review). *Oncol Rep*, *14*(6), 1583-1588. https://pubmed.ncbi.nlm.nih.gov/16273260

Katoh, M., & Katoh, M. (2007). Comparative integromics on non-canonical WNT or planar cell polarity signaling molecules: Transcriptional mechanism of PTK7 in colorectal cancer and that of SEMA6A in undifferentiated ES cells. *International Journal of Molecular Medicine*, *20*(3), 405-409. https://doi.org/10.3892/ijmm.20.3.405

Kaucká, M., Plevová, K., Pavlová, S., Janovská, P., Mishra, A., Verner, J., Procházková, J., Krejcí, P., Kotasková, J., Ovesná, P., Tichy, B., Brychtová, Y., Doubek, M., Kozubík, A., Mayer, J., Pospísilová, S., & Bryja, V. (2013). The planar cell polarity pathway drives pathogenesis of chronic lymphocytic leukemia by the regulation of B-lymphocyte migration. *Cancer Res*, *73*(5), 1491-1501. https://doi.org/10.1158/0008-5472.CAN-12-1752

Kimura, H., Usui, T., Tsubouchi, A., & Uemura, T. (2006). Potential dual molecular interaction of the Drosophila 7-pass transmembrane cadherin Flamingo in dendritic morphogenesis. *J Cell Sci*, *119*(Pt 6), 1118-1129. https://doi.org/10.1242/jcs.02832

Kohashi, K., Mori, Y., Narumi, R., Kozawa, K., Kamasaki, T., Ishikawa, S., Kajita, M., Kobayashi, R., Tamori, Y., & Fujita, Y. (2021). Sequential oncogenic mutations influence cell competition. *Curr Biol*, *31*(18), 3984-3995.e5. https://doi.org/10.1016/j.cub.2021.06.064

Kon, S., & Fujita, Y. (2021). Cell competition-induced apical elimination of transformed cells, EDAC, orchestrates the cellular homeostasis. *Dev Biol*, *476*, 112-116. https://doi.org/10.1016/j.ydbio.2021.03.015

Kon, S., Ishibashi, K., Katoh, H., Kitamoto, S., Shirai, T., Tanaka, S., Kajita, M., Ishikawa, S., Yamauchi, H., Yako, Y., Kamasaki, T., Matsumoto, T., Watanabe, H., Egami, R., Sasaki, A., Nishikawa, A., Kameda, I., Maruyama, T., Narumi, R., Morita, T., Sasaki, Y., Enoki, R., Honma, S., Imamura, H., Oshima, M., Soga, T., Miyazaki, J. I., Duchen, M. R., Nam, J. M., Onodera, Y., Yoshioka, S., Kikuta, J., Ishii, M., Imajo, M., Nishida, E., Fujioka, Y., Ohba, Y., Sato, T., & Fujita, Y. (2017). Cell competition with normal epithelial cells promotes apical extrusion of transformed cells through metabolic changes. *Nat Cell Biol*, *19*(5), 530-541. https://doi.org/10.1038/ncb3509

Lawrence, P. A., Casal, J., & Struhl, G. (2004). Cell interactions and planar polarity in the abdominal epidermis of Drosophila. *Development*, *131*(19), 4651-4664. https://doi.org/10.1242/dev.01351

Lee, R. C., Clandinin, T. R., Lee, C. H., Chen, P. L., Meinertzhagen, I. A., & Zipursky, S. L. (2003). The protocadherin Flamingo is required for axon target selection in the Drosophila visual system. *Nat Neurosci*, *6*(6), 557-563. https://doi.org/10.1038/nn1063

Leong, G. R., Goulding, K. R., Amin, N., Richardson, H. E., & Brumby, A. M. (2009). Scribble mutants promote aPKC and JNK-dependent epithelial neoplasia independently of Crumbs. *BMC Biol*, *7*, 62. https://doi.org/10.1186/1741-7007-7-62

Levayer, R., Dupont, C., & Moreno, E. (2016). Tissue Crowding Induces Caspase-Dependent Competition for Space. *Curr Biol*, *26*(5), 670-677. https://doi.org/10.1016/j.cub.2015.12.072

Levayer, R., Hauert, B., & Moreno, E. (2015). Cell mixing induced by myc is required for competitive tissue invasion and destruction. *Nature*, *524*(7566), 476-480. https://doi.org/10.1038/nature14684

Li, Y., Zhu, L., Hao, R., Li, Y., Zhao, Q., & Li, S. (2021). Systematic expression analysis of the CELSR family reveals the importance of CELSR3 in human lung adenocarcinoma. *J Cell Mol Med*, *25*(9), 4349-4362. https://doi.org/10.1111/jcmm.16497

Madan, E., Palma, A. M., Vudatha, V., Trevino, J. G., Natarajan, K. N., Winn, R. A., Won, K. J., Graham, T. A., Drapkin, R., McDonald, S. A. C., Fisher, P. B., & Gogna, R. (2022). Cell Competition in Carcinogenesis. *Cancer Res*, *82*(24), 4487-4496. https://doi.org/10.1158/0008-5472.CAN-22-2217

Madan, E., Pelham, C. J., Nagane, M., Parker, T. M., Canas-Marques, R., Fazio, K., Shaik, K., Yuan, Y., Henriques, V., Galzerano, A., Yamashita, T., Pinto, M. A. F., Palma, A. M., Camacho, D., Vieira, A., Soldini, D., Nakshatri, H., Post, S. R., Rhiner, C., Yamashita, H., Accardi, D., Hansen, L. A., Carvalho, C., Beltran, A. L., Kuppusamy, P., Gogna, R., & Moreno, E. (2019). Flower isoforms promote competitive growth in cancer. *Nature*, *572*(7768), 260-264. https://doi.org/10.1038/s41586-019-1429-3

Maruyama, T., & Fujita, Y. (2017). Cell competition in mammals - novel homeostatic machinery for embryonic development and cancer prevention. *Curr Opin Cell Biol*, *48*, 106-112. https://doi.org/10.1016/j.ceb.2017.06.007

Merino, M. M., Rhiner, C., Lopez-Gay, J. M., Buechel, D., Hauert, B., & Moreno, E. (2015). Elimination of unfit cells maintains tissue health and prolongs lifespan. *Cell*, *160*(3), 461-476. https://doi.org/10.1016/j.cell.2014.12.017

Merino, M. M., Rhiner, C., Portela, M., & Moreno, E. (2013). “Fitness fingerprints” mediate physiological culling of unwanted neurons in Drosophila. *Curr Biol*, *23*(14), 1300-1309. https://doi.org/10.1016/j.cub.2013.05.053

Meyer, S. N., Amoyel, M., Bergantiños, C., de la Cova, C., Schertel, C., Basler, K., & Johnston, L. A. (2014). An ancient defense system eliminates unfit cells from developing tissues during cell competition. *Science*, *346*(6214), 1258236. https://doi.org/10.1126/science.1258236

Morata, G. (2021). Cell competition: A historical perspective. *Dev Biol*, *476*, 33-40. https://doi.org/10.1016/j.ydbio.2021.02.012

Morata, G., & Calleja, M. (2020). Cell competition and tumorigenesis in the imaginal discs of Drosophila. *Semin Cancer Biol*, *63*, 19-26. https://doi.org/10.1016/j.semcancer.2019.06.010

Morata, G., & Ripoll, P. (1975). Minutes: mutants of drosophila autonomously affecting cell division rate. *Dev Biol*, *42*(2), 211-221. https://doi.org/10.1016/0012-1606(75)90330-9

Moreno, E. (2008). Is cell competition relevant to cancer. *Nat Rev Cancer*, *8*(2), 141-147. https://doi.org/10.1038/nrc2252

Moreno, E., & Basler, K. (2004). dMyc transforms cells into super-competitors. *Cell*, *117*(1), 117-129. https://doi.org/10.1016/s0092-8674(04)00262-4

Neto-Silva, R. M., de Beco, S., & Johnston, L. A. (2010). Evidence for a growth-stabilizing regulatory feedback mechanism between Myc and Yorkie, the Drosophila homolog of Yap. *Dev Cell*, *19*(4), 507-520. https://doi.org/10.1016/j.devcel.2010.09.009

Norman, M., Wisniewska, K. A., Lawrenson, K., Garcia-Miranda, P., Tada, M., Kajita, M., Mano, H., Ishikawa, S., Ikegawa, M., Shimada, T., & Fujita, Y. (2012). Loss of Scribble causes cell competition in mammalian cells. *J Cell Sci*, *125*(Pt 1), 59-66. https://doi.org/10.1242/jcs.085803

Ogawa, M., Kawarazaki, Y., Fujita, Y., Naguro, I., & Ichijo, H. (2021). FGF21 Induced by the ASK1-p38 Pathway Promotes Mechanical Cell Competition by Attracting Cells. *Curr Biol*, *31*(5), 1048-1057.e5. https://doi.org/10.1016/j.cub.2020.11.052

Ohsawa, S., Sugimura, K., Takino, K., Xu, T., Miyawaki, A., & Igaki, T. (2011). Elimination of oncogenic neighbors by JNK-mediated engulfment in Drosophila. *Dev Cell*, *20*(3), 315-328. https://doi.org/10.1016/j.devcel.2011.02.007

Pagliarini, R. A., & Xu, T. (2003). A genetic screen in Drosophila for metastatic behavior. *Science*, *302*(5648), 1227-1231. https://doi.org/10.1126/science.1088474

Parker, T. M., Gupta, K., Palma, A. M., Yekelchyk, M., Fisher, P. B., Grossman, S. R., Won, K. J., Madan, E., Moreno, E., & Gogna, R. (2021). Cell competition in intratumoral and tumor microenvironment interactions. *EMBO J*, *40*(17), e107271. https://doi.org/10.15252/embj.2020107271

Pérez, E., Lindblad, J. L., & Bergmann, A. (2017). Tumor-promoting function of apoptotic caspases by an amplification loop involving ROS, macrophages and JNK in Drosophila. *eLife*, *6*. https://doi.org/10.7554/elife.26747

Puvirajesinghe, T. M., Bertucci, F., Jain, A., Scerbo, P., Belotti, E., Audebert, S., Sebbagh, M., Lopez, M., Brech, A., Finetti, P., Charafe-Jauffret, E., Chaffanet, M., Castellano, R., Restouin, A., Marchetto, S., Collette, Y., Gonçalvès, A., Macara, I., Birnbaum, D., Kodjabachian, L., Johansen, T., & Borg, J. P. (2016). Identification of p62/SQSTM1 as a component of non-canonical Wnt VANGL2-JNK signalling in breast cancer. *Nat Commun*, *7*, 10318. https://doi.org/10.1038/ncomms10318

Rhiner, C., López-Gay, J. M., Soldini, D., Casas-Tinto, S., Martín, F. A., Lombardía, L., & Moreno, E. (2010). Flower Forms an Extracellular Code that Reveals the Fitness of a Cell to its Neighbors in Drosophila. *Developmental Cell*, *18*(6), 985-998. https://doi.org/10.1016/j.devcel.2010.05.010

Rosa, M., Noel, T., Harris, M., & Ladds, G. (2021). Emerging roles of adhesion G protein-coupled receptors. *Biochem Soc Trans*, *49*(4), 1695-1709. https://doi.org/10.1042/BST20201144

Sanchez Bosch, P., & Axelrod, J. D. (2024). Automated counting of Drosophila imaginal disc cell nuclei. *Biol Open*, *13*(2), bio060254. https://doi.org/10.1242/bio.060254

Schindelin, J., Arganda-Carreras, I., Frise, E., Kaynig, V., Longair, M., Pietzsch, T., Preibisch, S., Rueden, C., Saalfeld, S., Schmid, B., Tinevez, J.-Y., White, D. J., Hartenstein, V., Eliceiri, K., Tomancak, P., & Cardona, A. (2012). Fiji: an open-source platform for biological-image analysis. *Nature Methods*, *9*(7), 676-682. https://doi.org/10.1038/nmeth.2019

Senti, K. A., Usui, T., Boucke, K., Greber, U., Uemura, T., & Dickson, B. J. (2003). Flamingo regulates R8 axon-axon and axon-target interactions in the Drosophila visual system. *Curr Biol*, *13*(10), 828-832. https://doi.org/10.1016/s0960-9822(03)00291-4

Simons, M., & Mlodzik, M. (2008). Planar cell polarity signaling: from fly development to human disease. *Annual review of genetics*, *42*(1), 517-540. https://doi.org/10.1146/annurev.genet.42.110807.091432

Sreepada, A., Tiwari, M., & Pal, K. (2022). Adhesion G protein-coupled receptor gluing action guides tissue development and disease. *J Mol Med (Berl)*, *100*(10), 1355-1372. https://doi.org/10.1007/s00109-022-02240-0

Stowers, R. S., & Schwarz, T. L. (1999). A genetic method for generating Drosophila eyes composed exclusively of mitotic clones of a single genotype. *Genetics*, *152*(4), 1631-1639. https://doi.org/10.1093/genetics/152.4.1631

Struhl, G., Casal, J., & Lawrence, P. A. (2012). Dissecting the molecular bridges that mediate the function of Frizzled in planar cell polarity. *Development*, *139*(19), 3665-3674. https://doi.org/10.1242/dev.083550

Strutt, D., & Strutt, H. (2007). Differential activities of the core planar polarity proteins during Drosophila wing patterning. *Dev Biol*, *302*(1), 181-194. https://doi.org/10.1016/j.ydbio.2006.09.026

Strutt, H., & Strutt, D. (2008). Differential stability of flamingo protein complexes underlies the establishment of planar polarity. *Curr Biol*, *18*(20), 1555-1564. https://doi.org/10.1016/j.cub.2008.08.063

Suijkerbuijk, S. J., Kolahgar, G., Kucinski, I., & Piddini, E. (2016). Cell Competition Drives the Growth of Intestinal Adenomas in Drosophila. *Curr Biol*, *26*(4), 428-438. https://doi.org/10.1016/j.cub.2015.12.043

Sweeney, N. T., Li, W., & Gao, F. B. (2002). Genetic manipulation of single neurons in vivo reveals specific roles of flamingo in neuronal morphogenesis. *Dev Biol*, *247*(1), 76-88. https://doi.org/10.1006/dbio.2002.0702

Takechi, H., Hakeda-Suzuki, S., Nitta, Y., Ishiwata, Y., Iwanaga, R., Sato, M., Sugie, A., & Suzuki, T. (2021). Glial insulin regulates cooperative or antagonistic Golden goal/Flamingo interactions during photoreceptor axon guidance. *Elife*, *10*, e66718. https://doi.org/10.7554/eLife.66718

Tsachaki, M., & Sprecher, S. G. (2012). Genetic and developmental mechanisms underlying the formation of the Drosophila compound eye. *Developmental Dynamics*, *241*(1), 40-56. https://doi.org/10.1002/dvdy.22738

Uhlirova, M., & Bohmann, D. (2006). JNK- and Fos-regulated Mmp1 expression cooperates with Ras to induce invasive tumors in Drosophila. *EMBO J*, *25*(22), 5294-5304. https://doi.org/10.1038/sj.emboj.7601401

Usui, T., Shima, Y., Shimada, Y., Hirano, S., Burgess, R. W., Schwarz, T. L., Takeichi, M., & Uemura, T. (1999). Flamingo, a seven-pass transmembrane cadherin, regulates planar cell polarity under the control of Frizzled. *Cell*, *98*(5), 585-595. https://doi.org/10.1016/S0092-8674(00)80046-X

VanderVorst, K., Dreyer, C. A., Hatakeyama, J., Bell, G. R. R., Learn, J. A., Berg, A. L., Hernandez, M., Lee, H., Collins, S. R., & Carraway, K. L. (2023). Vangl-dependent Wnt/planar cell polarity signaling mediates collective breast carcinoma motility and distant metastasis. *Breast Cancer Res*, *25*(1), 52. https://doi.org/10.1186/s13058-023-01651-2

VanderVorst, K., Hatakeyama, J., Berg, A., Lee, H., & Carraway, K. L. (2018). Cellular and molecular mechanisms underlying planar cell polarity pathway contributions to cancer malignancy. *Semin Cell Dev Biol*, *81*, 78-87. https://doi.org/10.1016/j.semcdb.2017.09.026

Vincent, J. P., Fletcher, A. G., & Baena-Lopez, L. A. (2013). Mechanisms and mechanics of cell competition in epithelia. *Nat Rev Mol Cell Biol*, *14*(9), 581-591. https://doi.org/10.1038/nrm3639

Vishwakarma, M., & Piddini, E. (2020). Outcompeting cancer. *Nat Rev Cancer*, *20*(3), 187-198. https://doi.org/10.1038/s41568-019-0231-8

Vladar, E. K., Antic, D., & Axelrod, J. D. (2009). Planar cell polarity signaling: the developing cell's compass. *Cold Spring Harb Perspect Biol*, *1*(3), a002964. https://doi.org/10.1101/cshperspect.a002964

Wang, Y., Wang, H., Li, X., & Li, Y. (2016). Epithelial microRNA-9a regulates dendrite growth through Fmi-Gq signaling in Drosophila sensory neurons. *Dev Neurobiol*, *76*(2), 225-237. https://doi.org/10.1002/dneu.22309

Watanabe, H., Ishibashi, K., Mano, H., Kitamoto, S., Sato, N., Hoshiba, K., Kato, M., Matsuzawa, F., Takeuchi, Y., Shirai, T., Ishikawa, S., Morioka, Y., Imagawa, T., Sakaguchi, K., Yonezawa, S., Kon, S., & Fujita, Y. (2018). Mutant p53-Expressing Cells Undergo Necroptosis via Cell Competition with the Neighboring Normal Epithelial Cells. *Cell Rep*, *23*(13), 3721-3729. https://doi.org/10.1016/j.celrep.2018.05.081

Weeraratna, A. T., Jiang, Y., Hostetter, G., Rosenblatt, K., Duray, P., Bittner, M., & Trent, J. M. (2002). Wnt5a signaling directly affects cell motility and invasion of metastatic melanoma. *Cancer Cell*, *1*(3), 279-288. https://doi.org/10.1016/s1535-6108(02)00045-4

Wolff, T., & Ready, D. F. (1991). The beginning of pattern formation in the *Drosophila* compound eye: the morphogenetic furrow and the second mitotic wave. *Development*, *113*(3), 841-850. https://doi.org/10.1242/dev.113.3.841

Yamamoto, M., Ohsawa, S., Kunimasa, K., & Igaki, T. (2017). The ligand Sas and its receptor PTP10D drive tumour-suppressive cell competition. *Nature*, *542*(7640), 246-250. https://doi.org/10.1038/nature21033

Ziosi, M., Baena-López, L. A., Grifoni, D., Froldi, F., Pession, A., Garoia, F., Trotta, V., Bellosta, P., Cavicchi, S., & Pession, A. (2010). dMyc functions downstream of Yorkie to promote the supercompetitive behavior of hippo pathway mutant cells. *PLoS Genet*, *6*(9), e1001140. https://doi.org/10.1371/journal.pgen.1001140

Zuo, J., Zheng, A., Wang, X., Luo, Z., Chen, Y., Cheng, X., Zhao, Y., Zhou, X., Tang, K.-F., & Du, X. (2023). Upregulation of CELSR1 expression promotes ovarian cancer cell proliferation, migration, and invasion. *Medical Oncology*, *41*(1). https://doi.org/10.1007/s12032-023-02232-1

Figure 1

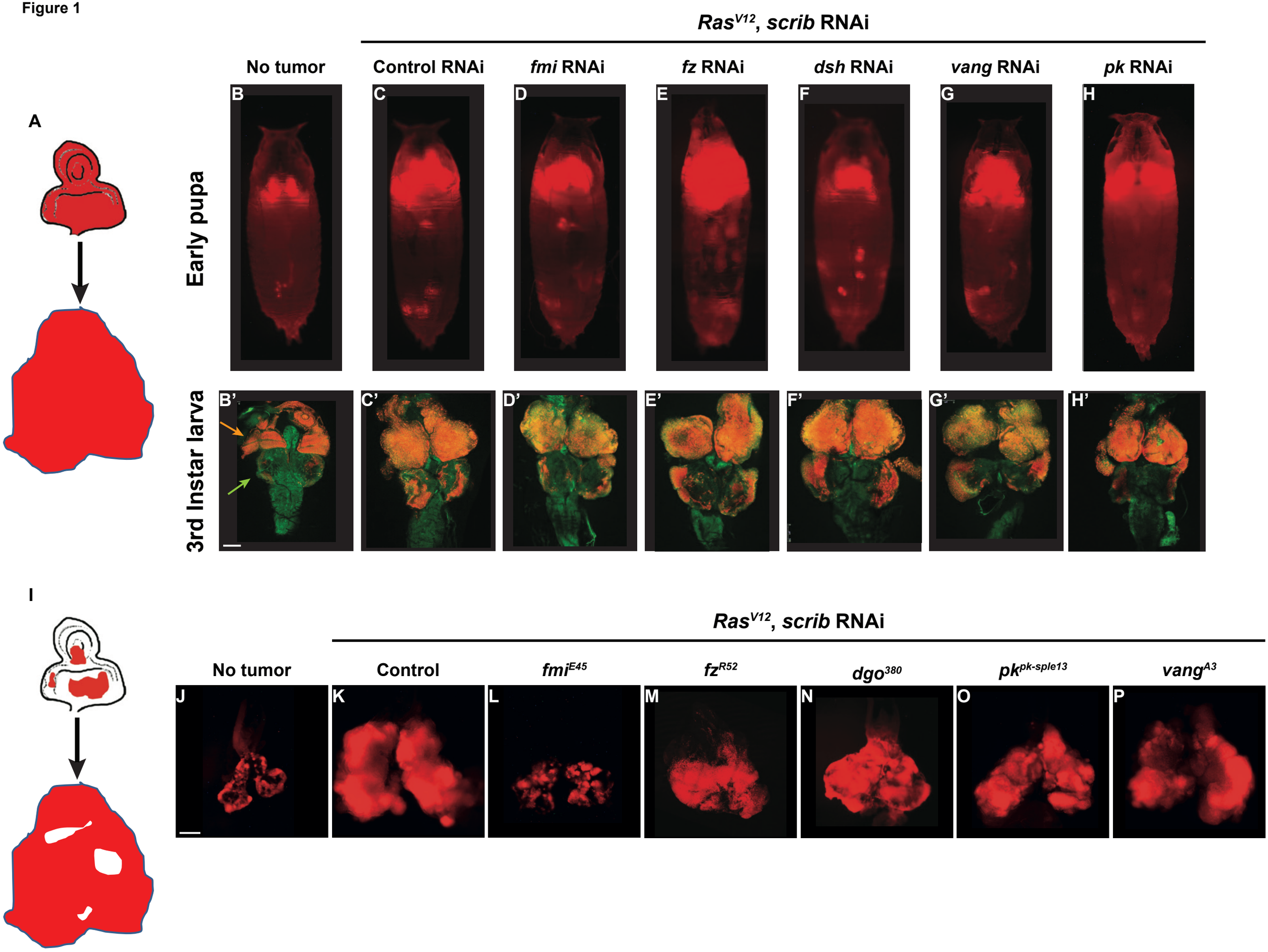
Ras^{V12}, scrib RNAi
No tumor
Control RNAi
fmi RNAi
fz RNAi
dsh RNAi
vang RNAi
pk RNAi
A
B
C
D
E
F
G
H
Early pupa
3rd Instar larva
B'
C'
D'
E'
F'
G'
H'
I
Ras^{V12}, scrib RNAi
No tumor
Control
fmi^{E45}
fz^{R52}
dgo^{380}
pk$^{pk\text{-}sple13}$
vang^{A3}
J
K
L
M
N
O
P

Figure 2

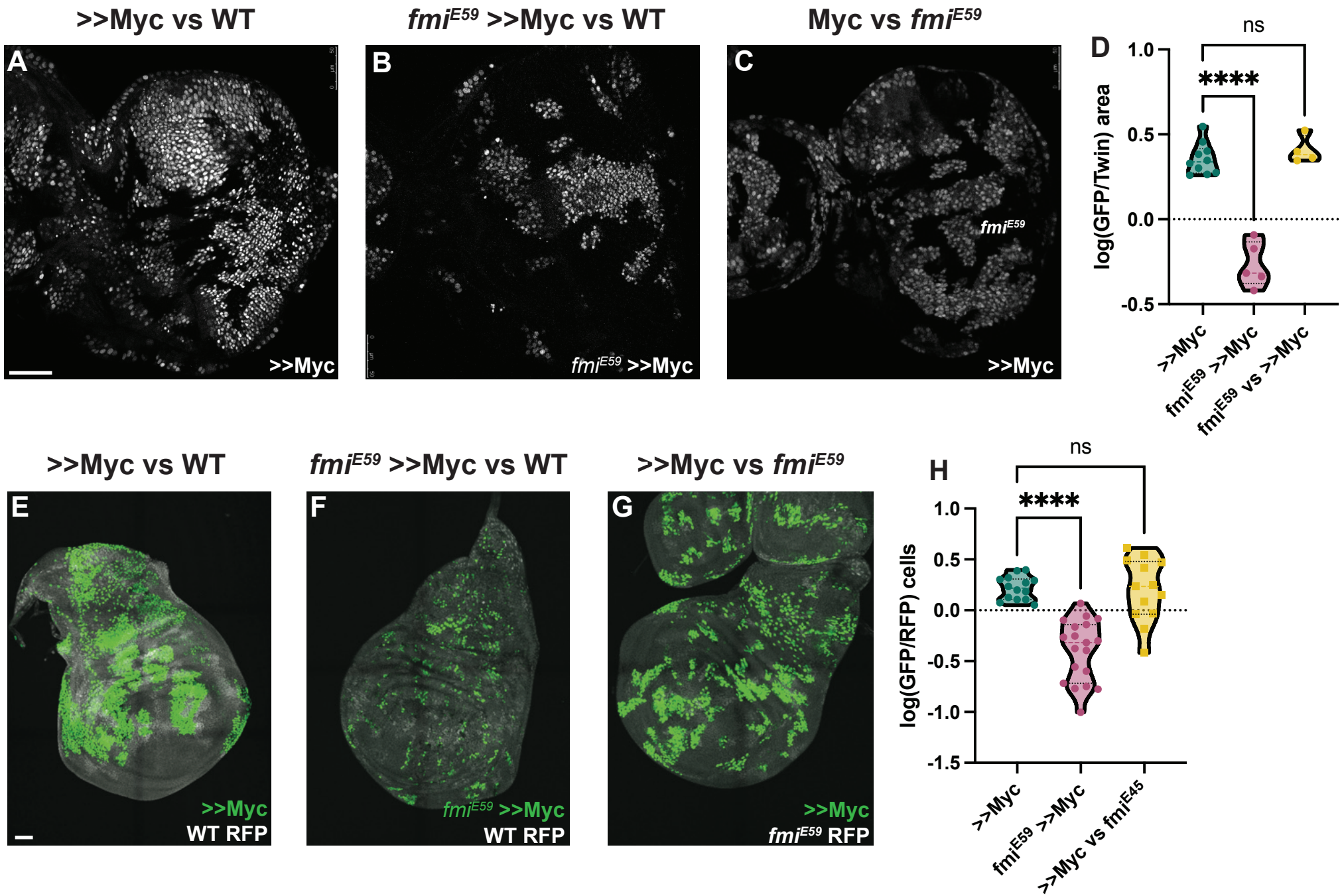
>>Myc vs WT
fmiE59 >>Myc vs WT
Myc vs fmiE59
A
>>Myc
B
fmiE59 >>Myc
C
fmiE59
>>Myc
D
ns
****
log(GFP/Twin) area
1.0
0.5
0.0
-0.5
>>Myc
fmiE59 >>Myc
fmiE59 vs >>Myc
>>Myc vs WT
fmiE59 >>Myc vs WT
>>Myc vs fmiE59
E
>>Myc
WT RFP
F
fmiE59 >>Myc
WT RFP
G
>>Myc
fmiE59 RFP
H
ns
****
log(GFP/RFP) cells
1.0
0.5
0.0
-0.5
-1.0
-1.5
>>Myc
fmiE59 >>Myc
>>Myc vs fmiE45

Figure 3

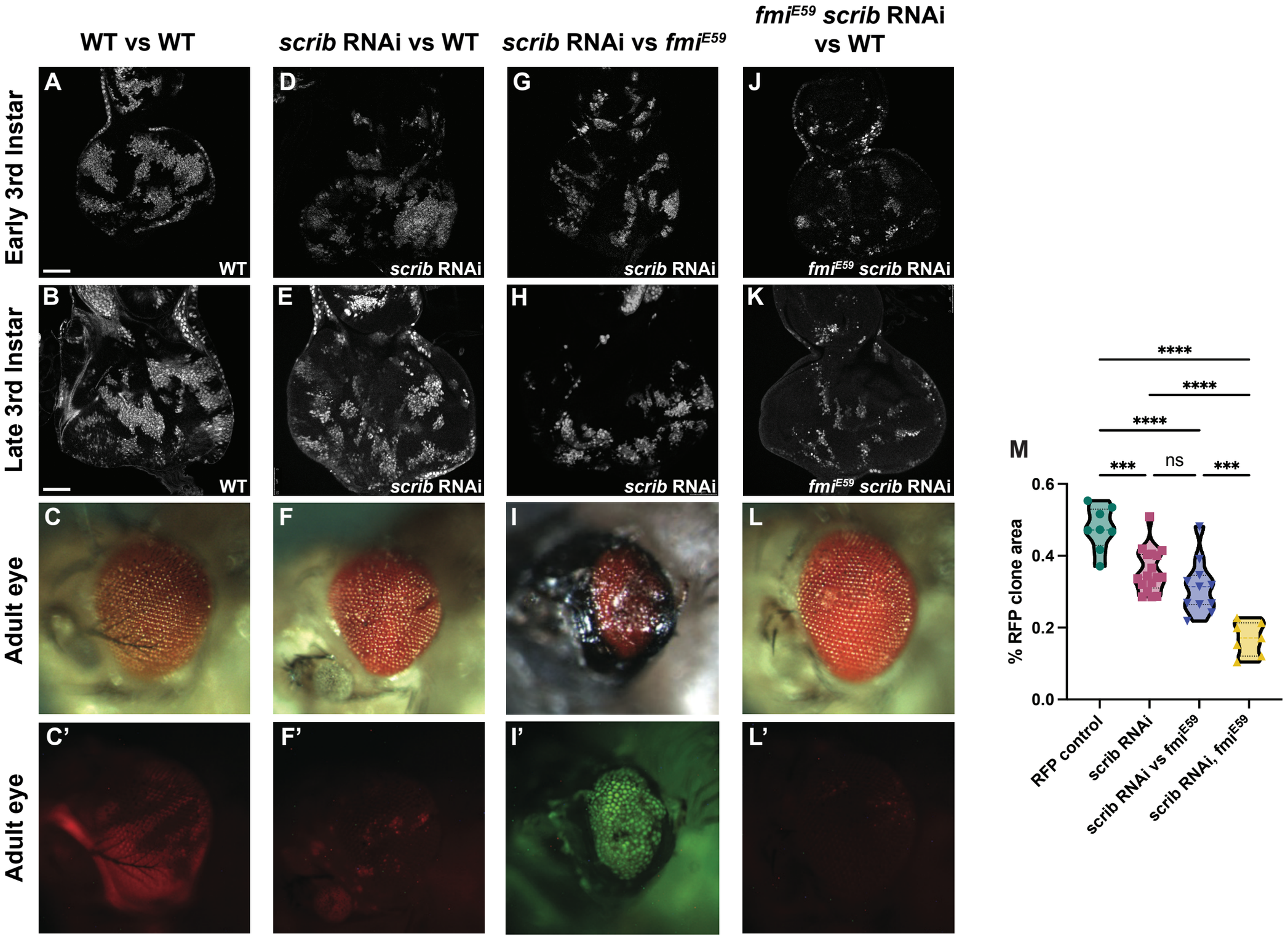
WT vs WT
scrib RNAi vs WT
scrib RNAi vs fmiE59
fmiE59 scrib RNAi vs WT
Early 3rd Instar
Late 3rd Instar
Adult eye
Adult eye
A
B
C
C'
D
E
F
F'
G
H
I
I'
J
K
L
L'
WT
scrib RNAi
fmiE59 scrib RNAi
M
% RFP clone area
0.0
0.2
0.4
0.6
****
****
****
***
ns
***
RFP control
scrib RNAi
scrib RNAi vs fmiE59
scrib RNAi, fmiE59

Figure 4

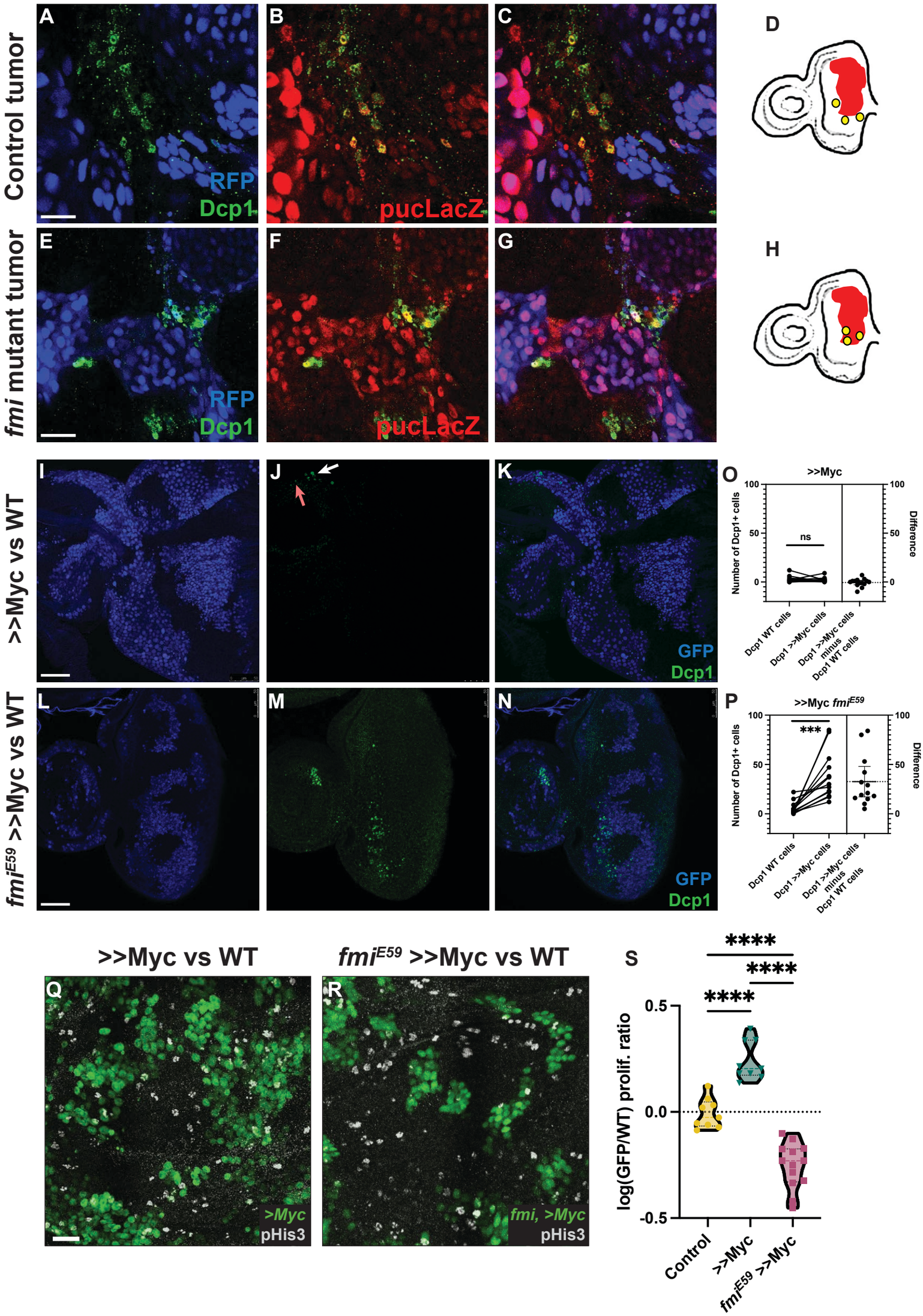
Control tumor
A
B
C
D
RFP
Dcp1
pucLacZ
fmi mutant tumor
E
F
G
H
RFP
Dcp1
pucLacZ
>>Myc vs WT
I
J
K
O
>>Myc
Number of Dcp1+ cells
Difference
ns
Dcp1 WT cells
Dcp1 >>Myc cells
Dcp1 >>Myc cells minus Dcp1 WT cells
GFP
Dcp1
fmiE59 >>Myc vs WT
L
M
N
P
>>Myc fmiE59
***
>>Myc vs WT
fmiE59 >>Myc vs WT
Q
R
S
>Myc
pHis3
fmi, >Myc
pHis3
****
****
****
log(GFP/WT) prolif. ratio
0.5
0.0
-0.5
Control
>>Myc
fmiE59 >>Myc

Figure 5

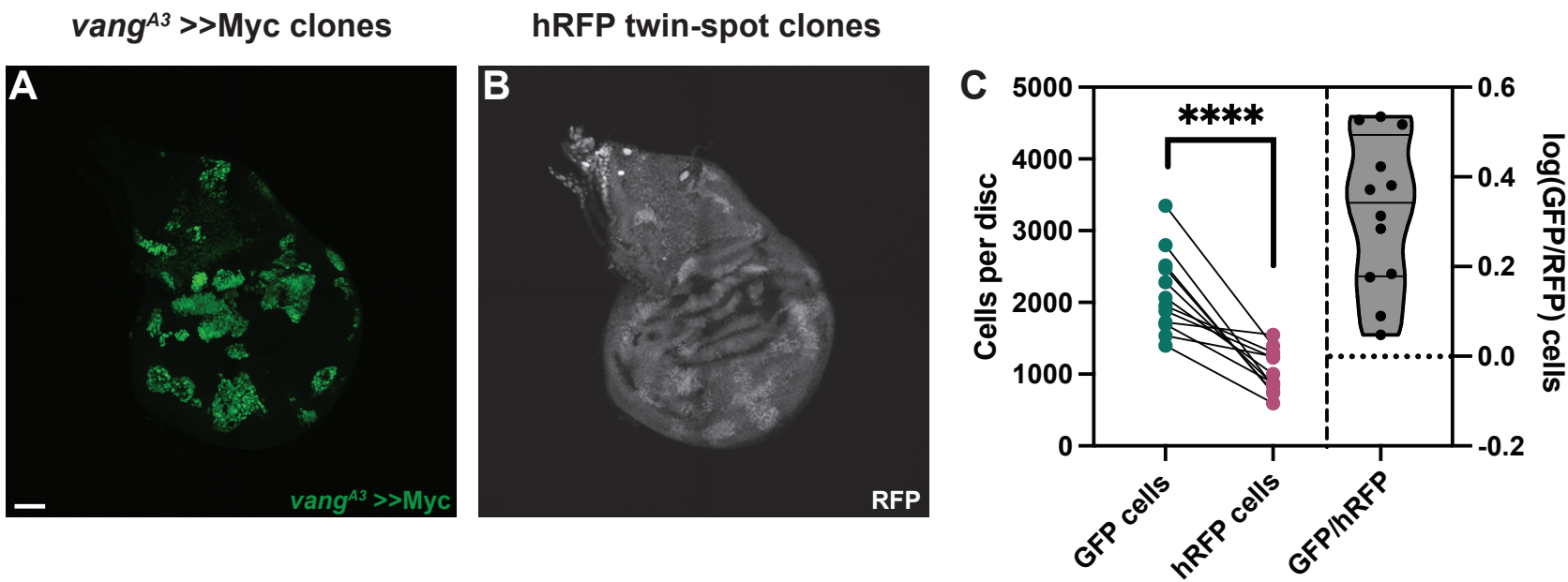
vang^A3 >>Myc clones
hRFP twin-spot clones
A
vang^A3 >>Myc
B
RFP
C
****
Cells per disc
5000
4000
3000
2000
1000
0
log(GFP/RFP) cells
0.6
0.4
0.2
0.0
-0.2
GFP cells
hRFP cells
GFP/hRFP

Figure 6

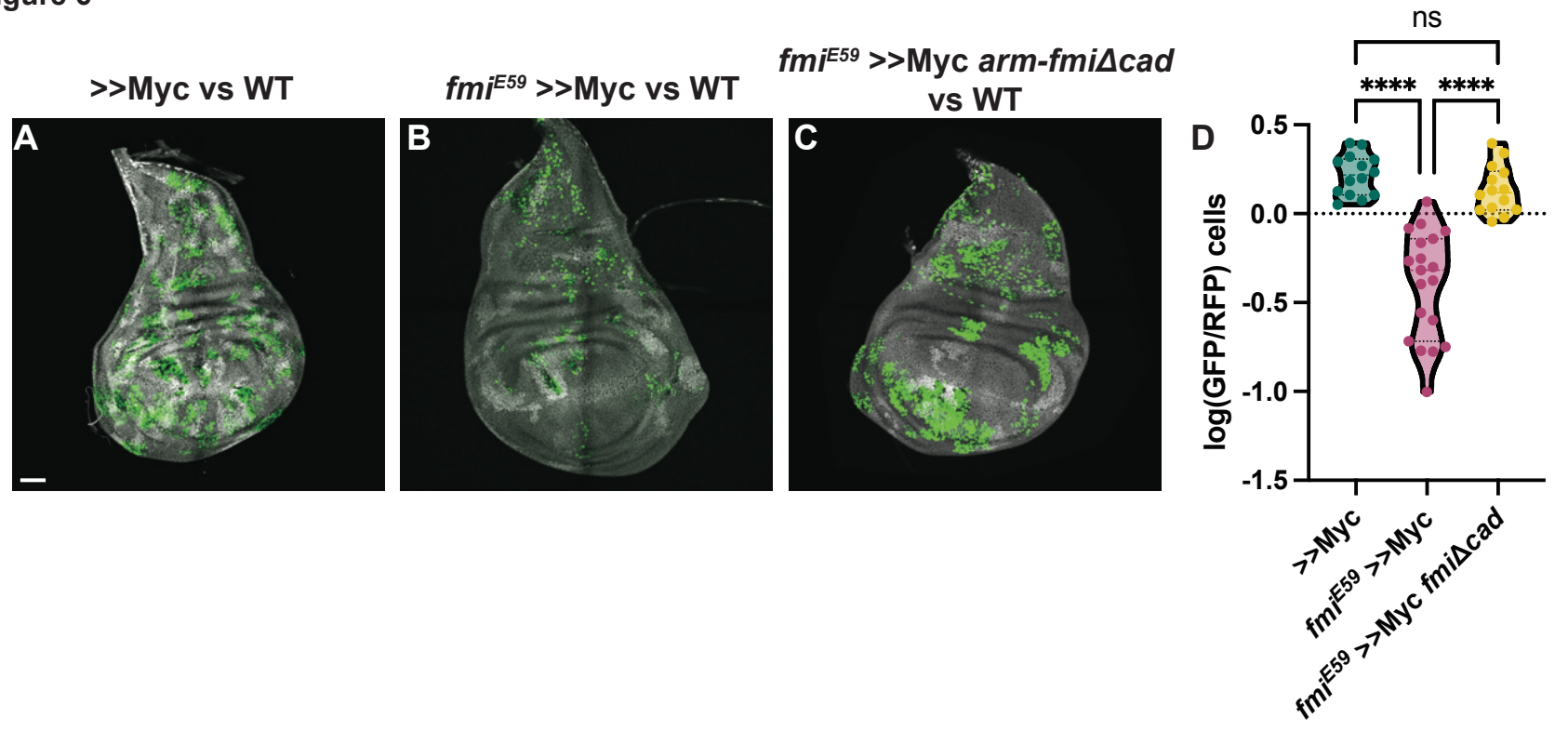
>>Myc vs WT
fmiE59 >>Myc vs WT
fmiE59 >>Myc arm-fmiΔcad vs WT
A
B
C
D
ns
****
****
0.5
0.0
-0.5
-1.0
-1.5
log(GFP/RFP) cells
>>Myc
fmiE59 >>Myc
fmiE59 >>Myc fmiΔcad

Figure 1 Supplement 1

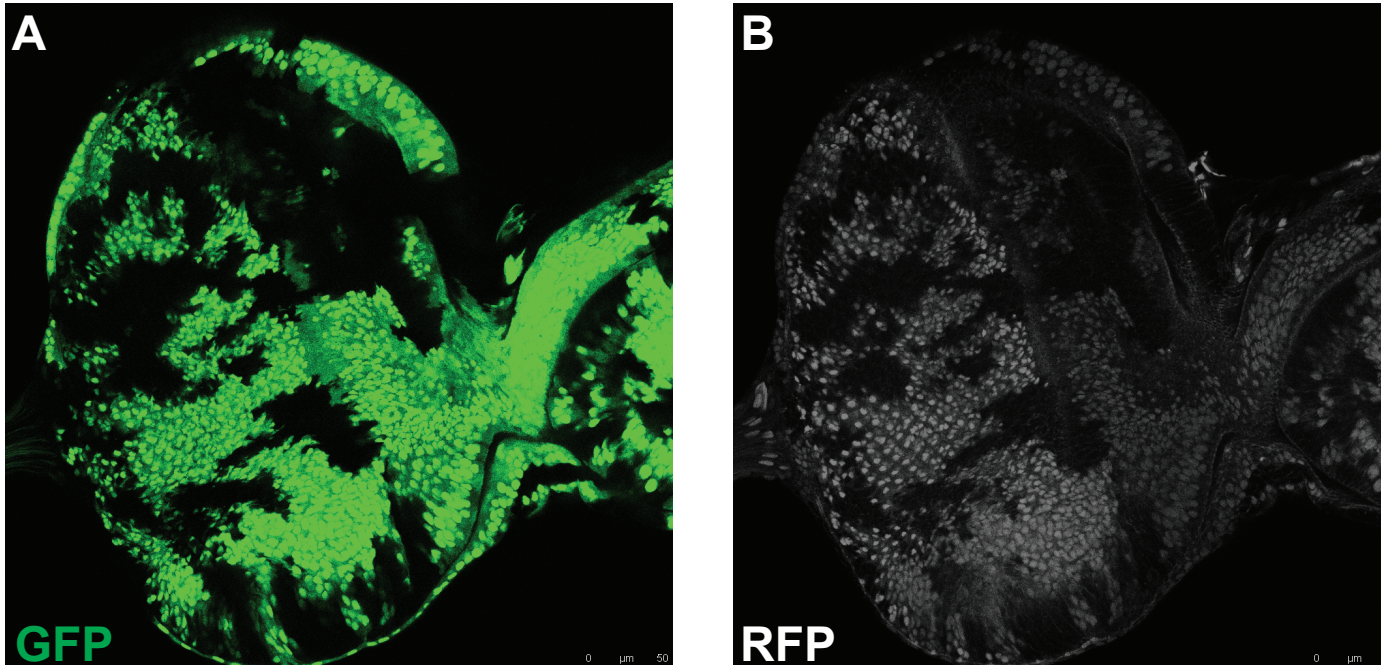

Figure 1 Supplement 2

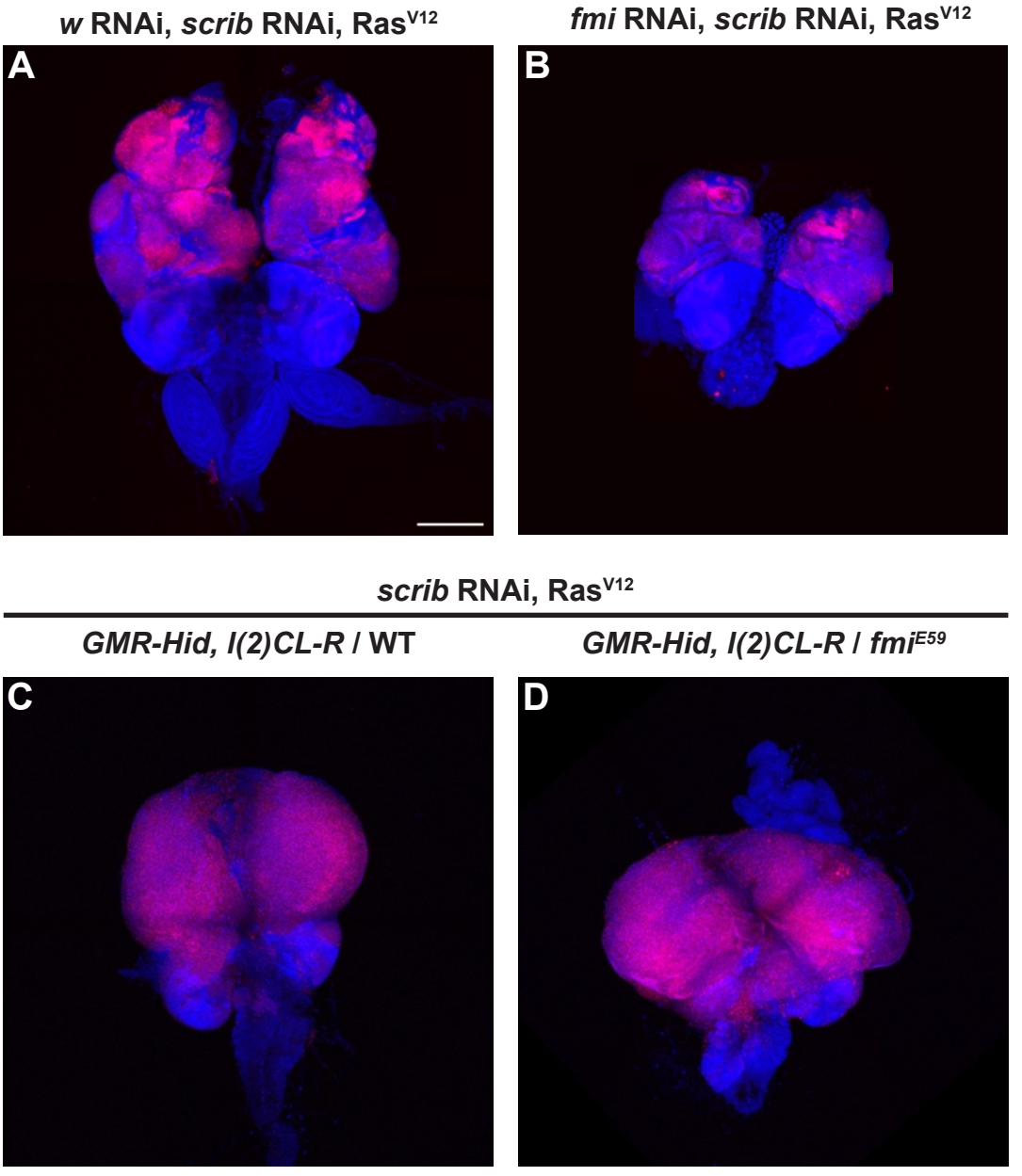

Figure 2 Supplement 1

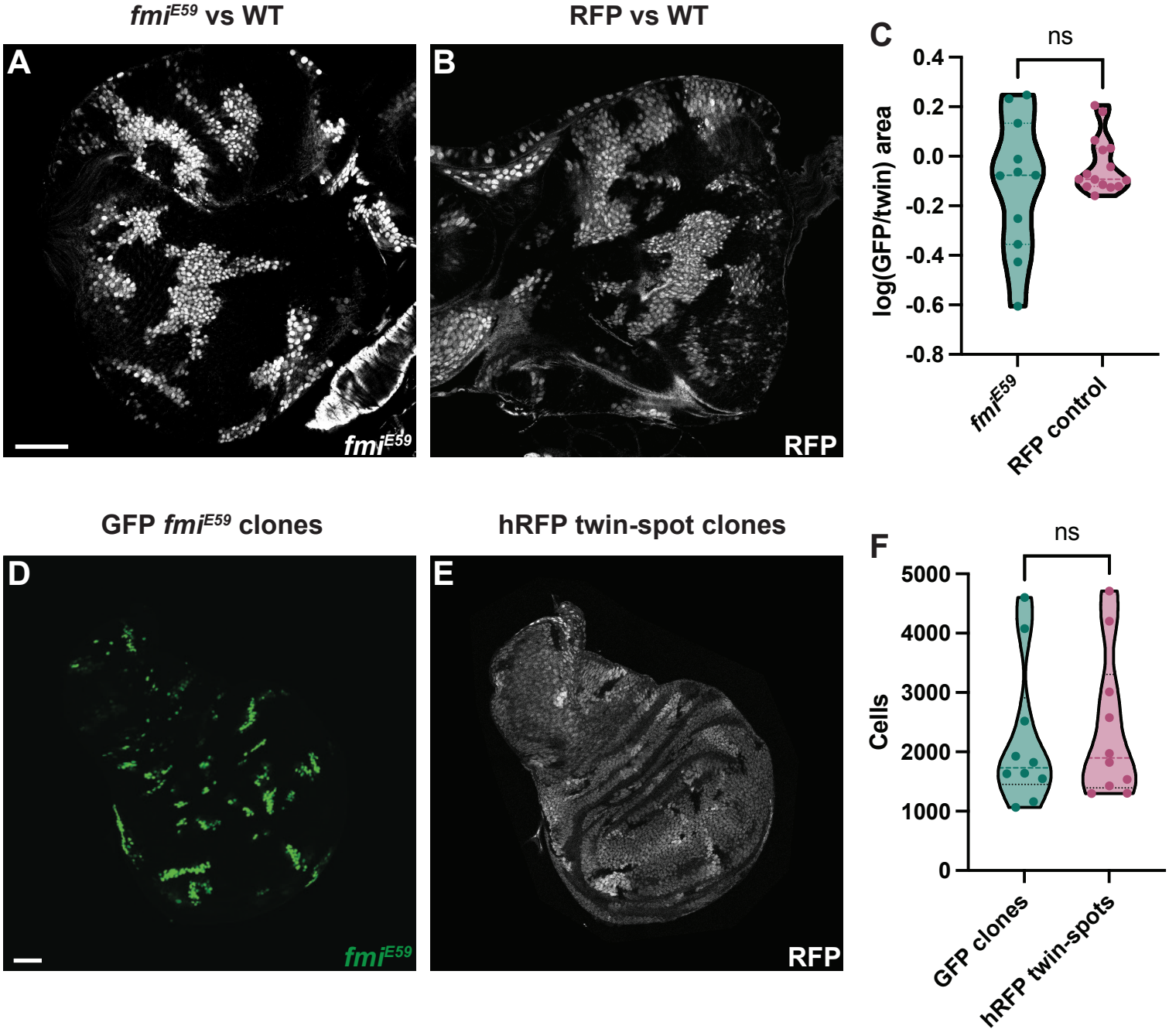

Figure 3 Supplement 1

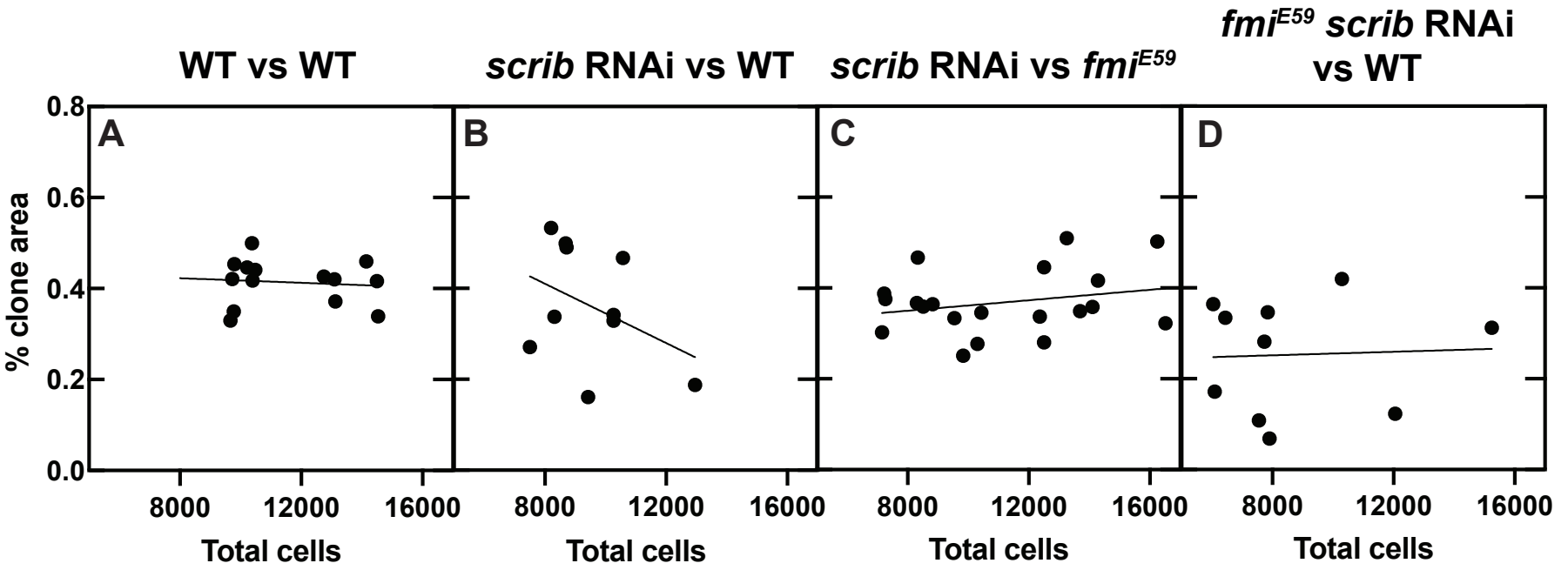

Figure 4 Supplement 1

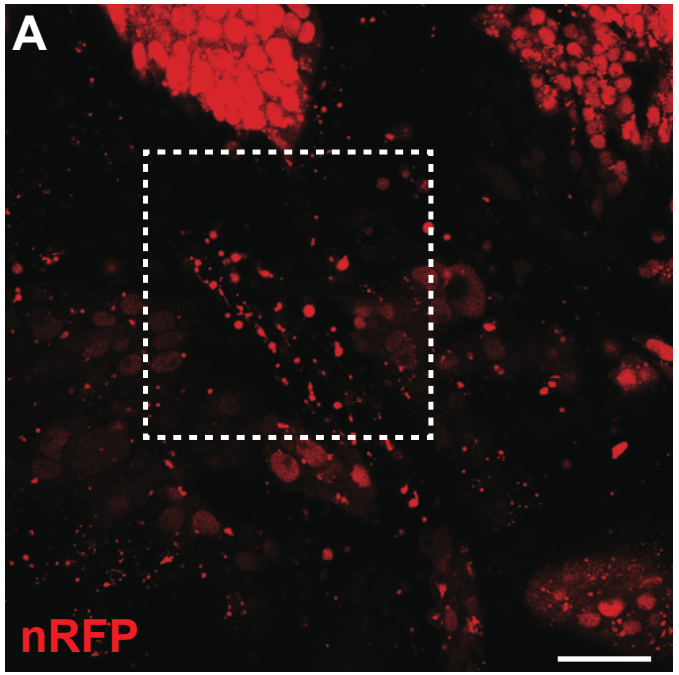

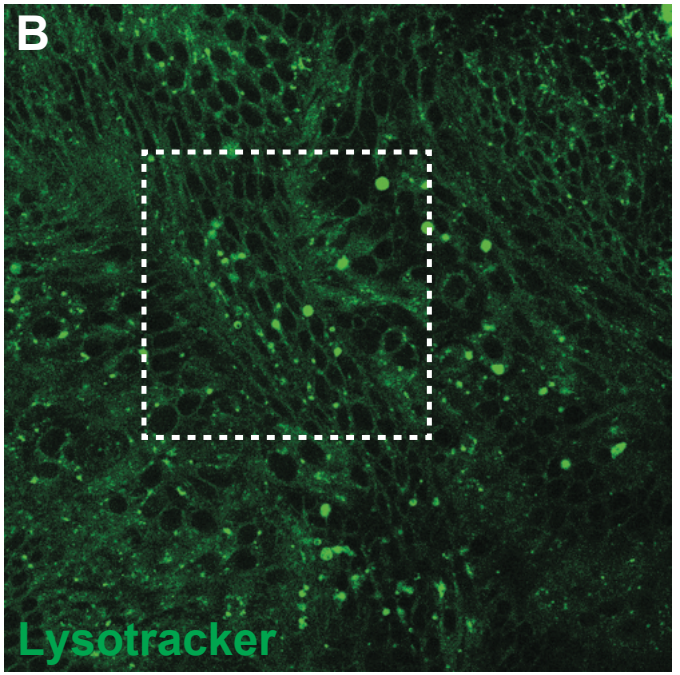

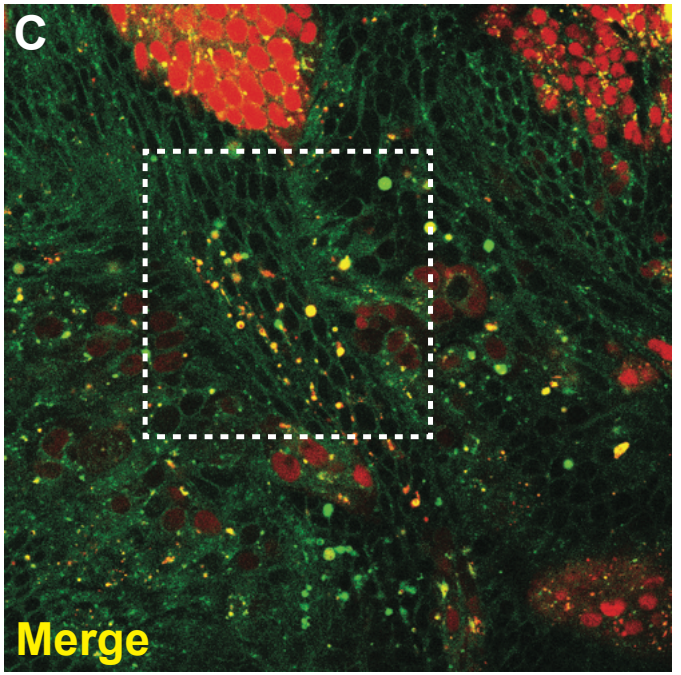

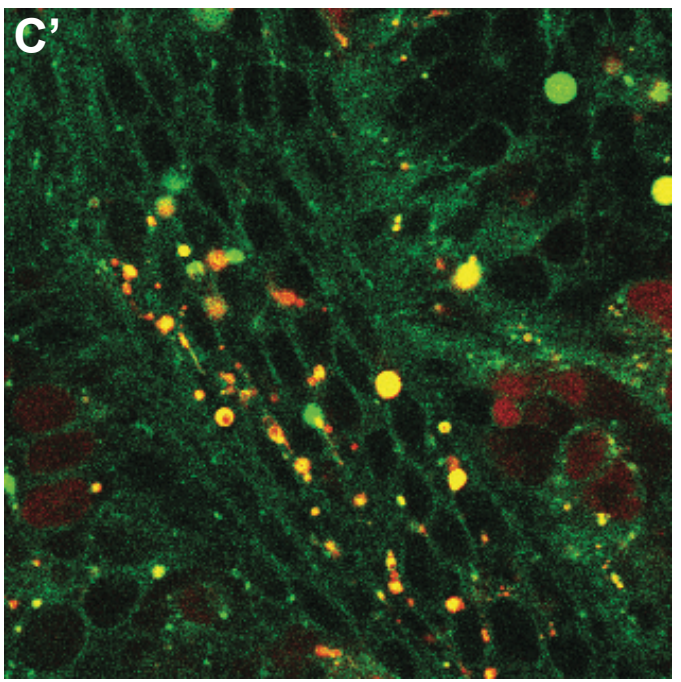

Figure 4 Supplement 2

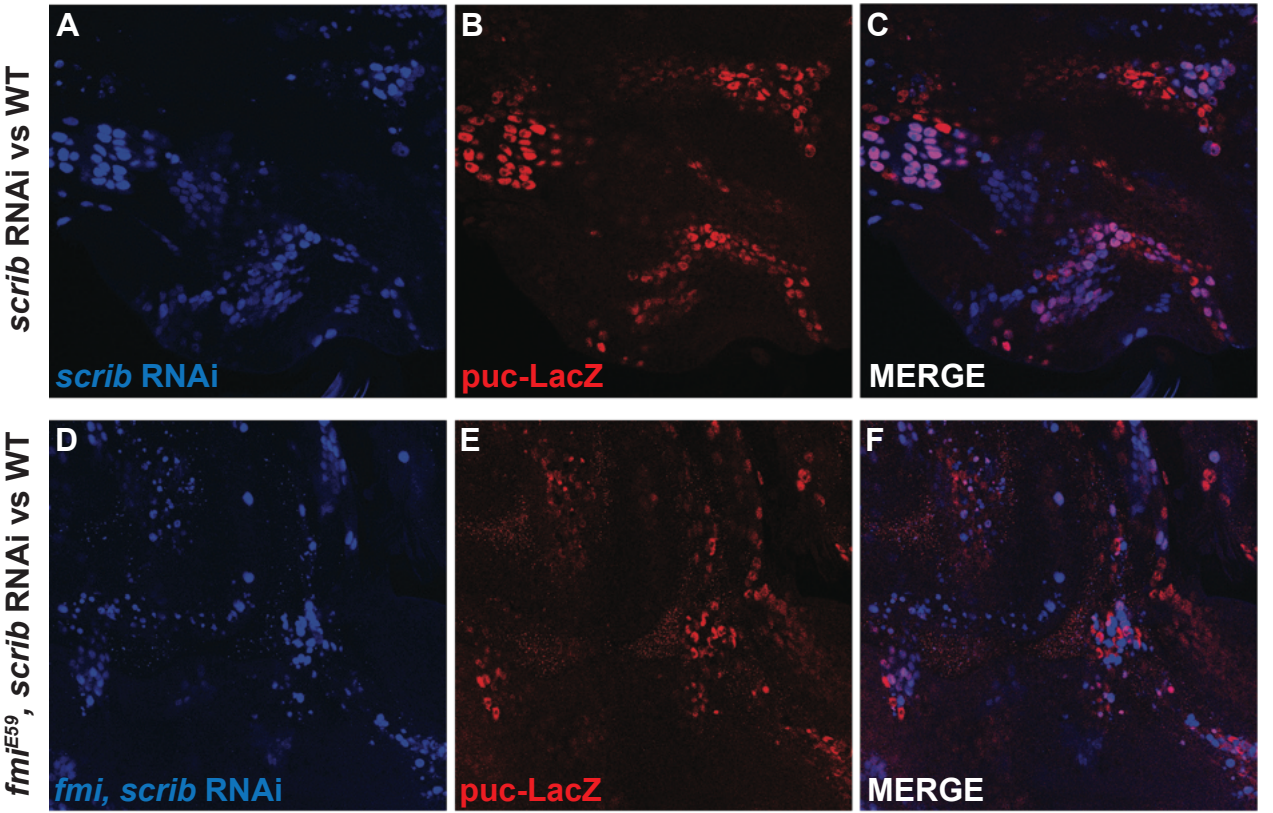
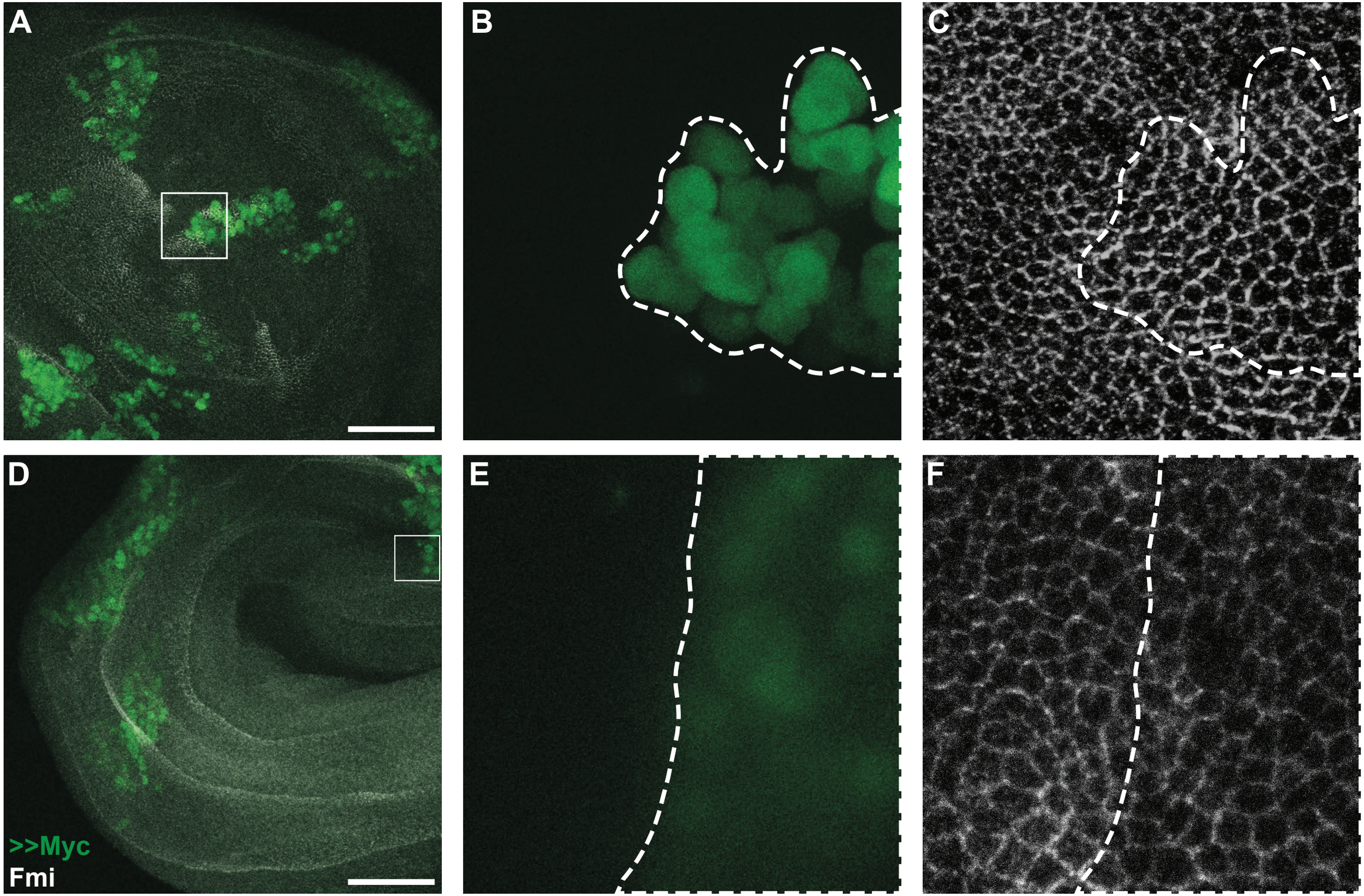
Figure 5 Supplement 1